DTU Civil Engineering
Department of Civil Engineering

MASTER THESIS

Modeling and simulation of the heat storage of a solar district heating plant

Author: Kilian Vicente Rubí (s212033)

Supervisor: Jianhua Fan

Co-supervisor: Simon Furbo

Technical University of Denmark (DTU)

Kongens Lyngby, Denmark
January, 2022

Acknowledgments

First of all, I would like to thank both my supervisor, Mr. Jianhua Fan, and my co-supervisor, Mr. Simon Furbo, for all of their support, guidance and advice during all these five months. Considering that it was a topic completely new for me and with hardly any background, thanks to them it has been a very fruitful and satisfying experience in which, above all, I consider that I have learned a lot, which is the most important thing for me.

I would also like to mention Xinyu Pan, a doctoral student who helped me selflessly to solve some problems that arose during the project.

And finally, I want to thank my family for all their unconditional support throughout my experience in Denmark. For always being there in the good times but especially when things were not going as I would like. Despite being far away from home, I have felt closer to them than ever.

Abstract

The aim of this study is to evaluate the long term performance of the water pit heat storage of the Dronninglund solar district heating plant in Denmark, located in the peninsula of Jutland. Experimental storage data from 2017 is evaluated, including the charged and discharged energy, its efficiency, the diffusers outlet temperatures, envelope heat losses and many more. In addition, simulation of different models are carried out based on Type 1535 and 1301 elements of TRNSYS, developed by TESS. The objective of these simulations is to analyze not only the long term performance of the storage, but the accuracy that the results have compared with the actual data. The differences between models are the number of layers in which the storage is divided, changes in geometry or modifications in soil properties to study how these changes affect to the performance of the storage. The results show that the models simulate with a pretty high accuracy the outlet temperatures of the storage, especially the ones from the top and bottom diffusers. The actual charged and discharged energy of the year in question is 11868 MWh and 11250 MWh, respectively. The simulations show a high accuracy in terms of charged energy, with only a -3% deviation in the worst case. Although the discharged energy is not as accurate as the charged energy, the results are quite acceptable. Total heat losses of the real storage have a value of 1157 MWh. The results of all models are deviate significantly from the actual value, both overestimated and underestimated, but the possible reasons are explained throughout this report. However, the distribution of the different types of heat losses among all models results in about 65% of top losses, 33% of edge losses and 2% of bottom losses, except in the model where the soil properties are modified, with a different percentage distribution. The same applies for the efficiency of the storage, whose actual value is 90%. The simulated efficiency values are higher for the models that with lower heat losses and lower values for the model with higher heat losses with respect to the real tank, since they are dependent parameters between them.

This study serves to draw some initial conclusions about how Type 1535 and Type 1301 perform as the water pit heat storage of Dronninglund.

Contents

Symbology

Latin symbols

Q	Energy [kJ]	D	Diameter [m]
$\dot{m}$	Mass flow [kg/h]	U	Heat transfer coefficient [W/(m²·K)]
C_p	Specific heat [kJ/(kg·K)]	St	Stratification coefficient [K²]
T	Temperature [°C]	K	Heat transferability [W/K]
V	Volume [m³]	A	Area [m²]
n	Number of nodes	Lcond	Conduction length [m]
M_E	Moment of energy [kJ·m]	Cap	Capacitance [kJ/K]
h	Convection coefficient [W/(m²·K)]	z	Vertical length [m]
Gr	Grashof number	r	Radial length [m]
H	Height [m]	R	Radius [m]
Pr	Prandtl number		
g	Acceleration of gravity [m/s²]		

Greek symbols

ρ	Density [kg/m³]	ν	Kinematic viscosity [m²/s]
η	Efficiency [%]	α	Thermal diffusivity [m²/day]
λ	Thermal conductivity [W/(m·K)]	δ	Thickness [m]
μ	Dynamic viscosity [kg/(m·s)]	Δ	Difference
β	Thermal expansion coefficient [1/K]	τ	Time [s]

Abbreviations

TES	Thermal Energy Storage	HDPE	High-Density Polyethylene
PTES	Pit Thermal Energy Storage	MIX	MIX number
STES	Seasonal Thermal Energy Storage	HX	Heat Exchanger
SDH	Solar District Heating		

Subscripts

ch	Charge	min	Minimum
disch	Discharge	geo	Geotextile liner
in	Inlet flow	side	Side of the storage
out	Outlet flow	ins	Insulation
loss	Heat losses	soil	Surrounding soil
top	Top diffuser	r	Radial direction
middle	Middle diffuser	z	Vertical direction
bot	Bottom diffuser		
av	Average		
w	Water		
max	Maximum		

1. Introduction

The continued increase in fossil fuel energy consumption has led to the need to shift towards renewable energy solutions, i.e. clean energy sources that do not contribute to climate change. That is why in Denmark, the investment in renewable energy is to meet the Danish government's aim to be independent of fossil fuels by 2050 (Danish Energy Agency, Danish Ministry of Climate, Energy and Utilities [1]).

Despite the fact that Denmark receives low radiation throughout the year, solar energy plays an important role in generating electricity and heat. After wind energy, solar energy is one of the most important renewable sources in the country and that is therefore a promising renewable source to replace the use of fossil fuels. For this reason, the study and evaluation of solar district heating plants has experienced a boom in recent years (Tulus et al., 2016 [2]).

Heat supply in Denmark can be either individual (20%) or collective (80%). Individual heat supply is characteristic of rural areas and small towns which are outside of the district heating zones. These district heating areas take care of collective heat supply by distributing the hot water from a central district heating plant to the individual buildings. 2/3 of Danish houses are heated by such a system. Another form of collective heating supply is natural gas which, through a distribution network formed by gas pipes and an individual gas boiler in each building, provides heat and hot water (Danish Energy Agency, Danish Ministry of Climate, Energy and Utilities [1]).

Returning to solar energy as a source of heat production, it presents a clear mismatch between production and demand, as it suffers significant daily and seasonal fluctuations. Therefore, it is necessary to store the energy produced. Moreover, since the season in which the energy produced is higher is the same season in which the demand is lower, it leads to believe that thermal energy storage has a very important role to play in the future of this renewable energy source.

Nowadays, thermal energy storage (TES) is one of the most important storage technologies. This type of storage technology helps solve the mismatch between production and demand as it has the ability to store surplus of solar energy and make it available when needed. There are several types of TES or also called STES (Seasonal Thermal Energy Storage)

depending on their shape and the hydrogeological conditions of the site where they are able to be built (Ochs et al., 2009 [3]). The most common are borehole thermal energy storage (BTES), aquifer thermal energy storage (ATES), pit thermal energy storage (PTES), tank thermal energy storage (TTES) and cavern thermal energy storage (CTES) (Dahash et al., 2019 [4]).

This project is going to focus on the study of a particular PTES, which belongs to the Dronninglund solar district heating plant. The study consists of using the TRNSYS elements developed by TESS (types 1535 and 1301) to simulate the behavior of an inverted truncated cone-shaped water pit heat storage and its surrounding ground for modeling in order to compare the simulation results with the experimental data of the real tank. In this case, parameters such as charged and discharged energy, outlet and average temperatures, envelope heat losses and thermal stratification are analyzed to evaluate the performance of the models in relation to the 2017 experimental data

Other similar studies have served as guidance for the realization of this project. The report developed by Gauthier in 2020 [5] includes the simulation of three components developed for TRNSYS. The first and simplest is type 342, which consists of a cylindrical shaped storage with vertical walls and was developed by TransSolar. The second, developed by Natural Resources Canada and TESS, is composed of two elements that are called types 1300 and 1301. Type 1300 is a prequel to the component that is studied in this project (type 1535) and has an inverted truncated cone shape, while type 1301 simulates the behavior of the surrounding soil. Finally, a truncated pyramid model called type 1322 was developed by TESS exclusively for PlanEnergi and SOLITES. All TRNSYS elements have in common that the simulation of storage behavior is in one dimension. The soil simulation in all models is in two dimensions, except for type 1322, which is the most sophisticated and simulates it in three dimensions. Another similar and more recent study of this type is by Xie et al. in 2021 [6], where they analyze the TRNSYS component called type 343 developed by ICEPIT. This component also has an inverted truncated cone shape and the storage and the soil are simulated in 1D and 2D, respectively.

2. Dronninglund solar district heating plant

Dronninglund SDH plant provides almost half of heat demand of the danish town of Dronninglund. The operation of this plant is based on both seasonal and short-term heat storage and it is mainly formed by a 37573 m^2 solar collectors field, a 60000 m^3 water pit heat storage, an absorption heat pump and a 46 km district heating pipes network. In summer, inlet and outlet temperatures of the solar collector field can reach 40 / 80 - 90 ºC respectively and, in cold season, both temperatures drop until 15-20 / 30-40 ºC . The demand temperature is about 75 ºC while the return water has a temperature of 40 ºC before going back to the storage. A simplified scheme of the SDH is depicted on Figure 1. As in non-heating season the energy generated by the system is higher than the required, the surplus is used to heat the upper part of the storage until 90 ºC. This temperature was set to this value to maintain an enough lifetime of the liner that surrounds the PTES. The main function of the absorption heat pump is to supply the corresponding demand in case the top temperature of the storage is lower than the required. Other great advantage of the heat pump is to use it to cool down the return water to 10 ºC. This affects positively the efficiency of the system because with the increase of temperatures inside the storage, the capacity, i.e. the energy stored increase with the same volume. Heat losses reduce due to the increasing of average temperature of the storage. It does not only affect to the efficiency of the storage but the efficiency of the solar collectors field increases because the operation temperatures are lower.

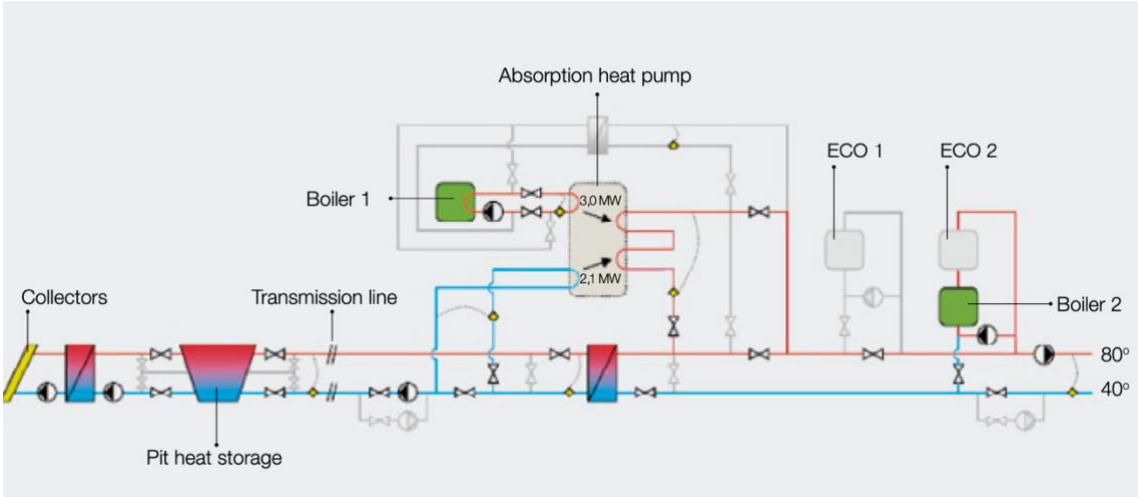

Figure 1. Diagram of Dronninglund Solar district Heating Plant (PlanEnergi, 2015 [7])

2.1 The water pit heat storage

The water pit was built in an abandoned gravel pit (Figure 2). A geological study from 2011 (PlanEnergi, 2011 [8]) determined that from the soil surface to 27 m depth it is mainly formed by dry sand, while, from this depth, the soil is water-saturated. The PTES has a volume of 60000 m^3 and has a shape of an inverted truncated pyramid with a height of 16 m. The upper side has a length of 90 m and the bottom side of 26 m. The slope of the storage is fixed on 26.6º. The top surface is covered by a flexible lid made of 3 layers of *Normalén* and each with a thickness of 80 mm, i.e. 240 mm in total (Gauthier, 2020 [5]). The rest of the structure is surrounded by a 2.5 mm HDPE liner and a very thin layer of geotextile (Jensen, 2014 [9]). Between the upper cover and the top surface of the PTES there is an air gap which its aim is to remove the moisture through ventilation (Figure 3). There is also a weight pipe over the cover that helps to remove the rainwater and its objective is to lead the rainwater from all the spots of the cover to the center where a pump will remove it to keep the floating line in good condition (Figure 4).

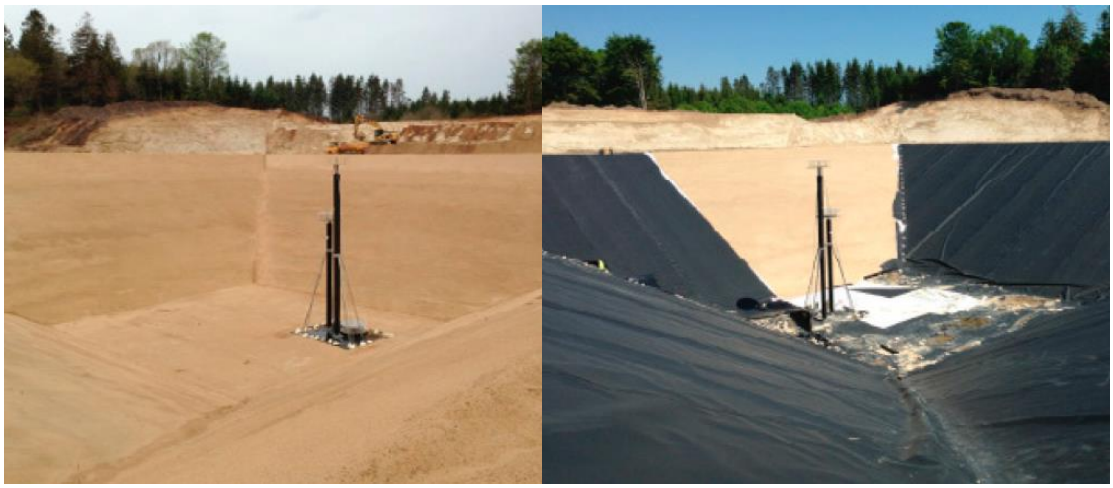

Figure 2. Construction of the water pit heat storage

The water flow enters and exits the PTES through the bottom of the storage tank. Once inside the storage, there are three pipes that each ends with a diffusor located on top, bottom and in the volumetric center of the storage, i.e. in a position where half of the water volume is above and the other half below (Gauthier, 2020 [5]). All three pipes are used at the same time to ensure a good operation of the PTES. For example, if the water coming from the solar array has a lower temperature than that of the top layer, it can be introduced through the middle diffuser to favor the thermal stratification phenomena.

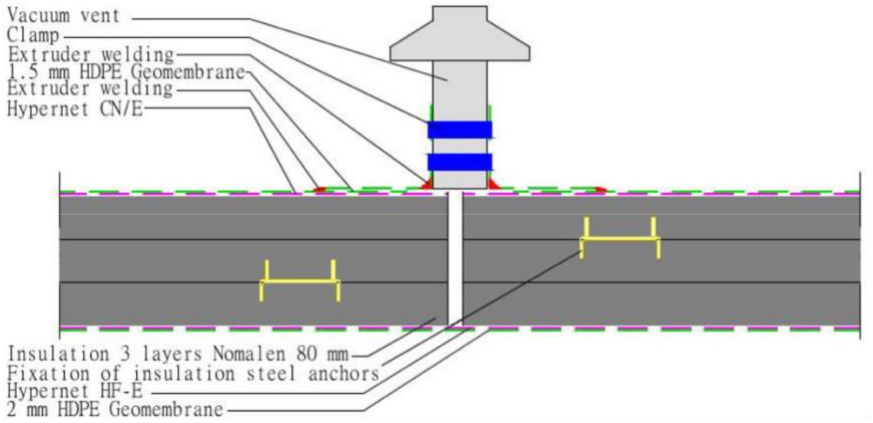

Figure 3. Ventilation device to remove moisture from the surface of the PTES

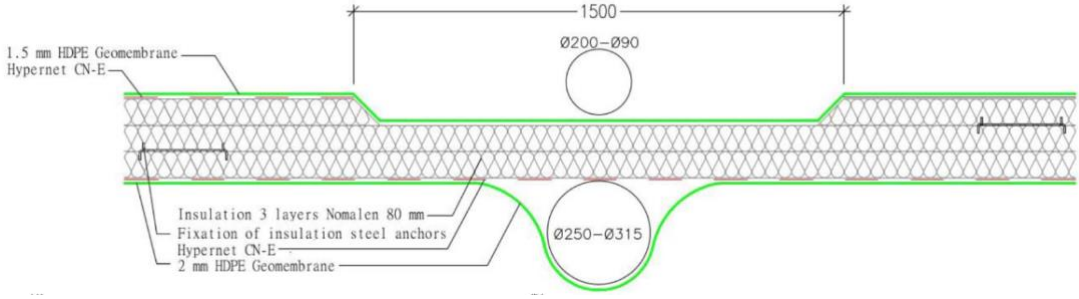

Figure 4. Cross section of the tank cover water drainage system

3. PTES measurements

The measurements of the PTES are obtained thanks to a series of sensors that have been installed both inside the storage and the surrounding area. These data include temperatures inside the PTES (lid insulation, water and pipes), ambient temperature and volume flowrate. There are 32 temperature sensors inside the tank distributed every 0.5 m from the bottom to the top except the top one that is located 0.1 m below the lid insulation. There are also two more temperature sensors installed on the top and the bottom of the cover. In addition, three temperature sensors have been placed on each pipe that leads to the diffusers. Apart from the temperature measurement, there is also a flowmeter installed on each pipe to measure both flowrate direction (inlet/outlet) and magnitude. It should be noted that the flow data is made assuming a volumetric flow. All the data is recorded with a timestep of 10 minutes from the first day of the year until the last one.

In order to properly calibrate the TRNSYS model, data from a year prior to the year under study can be used as initial conditions to obtain more accurate results after the simulation. If the objective is to simulate more than one year, the process can be carried out in the same way as explained above.

3.1 Experimental results

There is some data from the measurement that we can use directly to compare with the results obtained on the simulation such as the distribution temperature in the storage, the temperature on each diffuser and the heat losses through the top cover. Since there are 32 temperature sensors, the real temperatures to compare with the diffusers outlet temperatures are the ones corresponding to the data delivered by sensor number 31 (top diffuser), sensor number 24 (middle diffuser) and sensor number 1 (bottom diffuser). On the other hand, to obtain other interesting results is needed to make some calculations. Precisely, to calculate the energy charged and discharged during a year an energy balance is used *(1)* in each time step. Is decided to use an energy balance because the model uses a similar equation to calculate the energy delivered to each port.

$$Q_{ch/disch} = \dot{m} \cdot C_P \cdot (T_{out} - T_{in}) \quad (1)$$

To make it simpler and as it has been explained before, it is assumed that the mass flow is considered the same for the inlet and the outlet. The specific heat is assumed to be constant during all the simulation because like this is how the model consider the properties of water.

The content of energy in the storage is also an important parameter. This is calculated as the equation *(2)* describes, with the properties of the water considered constant.

$$Q_{storage} = \sum_{i=1}^{N} \rho \cdot C_p \cdot V_i \cdot T_i \quad (2)$$

Taking advantage of both previous expressions, experimental heat losses can be calculated. Considering the storage as a control volume, the energy balance *(3)* that describes its inlets, outlets and intern changes allows to obtain the total heat losses during the year of study.

$$Q_{losses} = (Q_{ch} - Q_{disch}) - \Delta Q_{storage} \quad (3)$$

Where the $\Delta Q_{storage}$ is the internal change of the energy content, calculated as the difference between the energy content at the final time step and the energy content inside the storage at the beginning of the year. If this value is negative it means that the storage would have lost internal energy due to changes on layers temperature.

4. Validation of the model

In order to consider a good model of the PTES, two kinds of analysis will be done. One analysis consist on study the accuracy of the model through the coefficient of determination applied on different parameters to see whether the model's behavior is similar to the one of the real storage or not and in which grade it is. The other important analysis is the study of the performance of the PTES which can be evaluated through the thermal stratification, the storage efficiency and the capacity of the storage. This can be useful for design parameters of the PTES such as the emplacements of the pipes or control strategies. It has to be said that different models will be studied in order to see how affects the parameters of each model to the accuracy and the performance of the PTES.

4.1 Model accuracy – Coefficient of determination R^2

As mentioned before, the coefficient of determination is an indicator to evaluate the model accuracy. It indicates how the model is replicating a certain experimental data during all the simulation. This coefficient is calculated as equations *(4)*, *(5)*, *(6)* and *(7)* describe and can reach values from 0 to 1, where the closer to 1 the more accurate is the model. The critical variables analyzed with this method are the outlet temperatures in each diffuser and the annual charged and discharged energy. Heat losses from top, edges and bottom are also potential variables to be analyzed with this criteria but, since the measurement data just offer lid losses it has been decided not to include them. Total heat losses from the measurement data can be calculated with *(3)* and analyzed using this method but the fact that is a variable that oscillates as much as the measurements can make the model less reliable than it actually is (Gauthier, 2020 [5]).

$$R^2 = 1 - \frac{S_{res}}{S_{total}} \tag{4}$$

$$S_{res} = \sum_i (y_i - x_i)^2 \tag{5}$$

$$S_{total} = \sum_i (y_i - \bar{y})^2 \tag{6}$$

$$\bar{y} = \frac{1}{n} \sum_i y_i \tag{7}$$

Where y_i is the experimental variable and x_i is the simulated variable in each time step. This method is used to compare the accuracy of all the models from this project in order to evaluate which one is the best in terms of model accuracy. The global coefficient of determination is described on equation *(8)*, which exclude heat losses for the reason explained before.

$$R^2{}_{global} = \frac{R^2{}_{top,T} + R^2{}_{middle,T} + R^2{}_{bottom,T} + R^2{}_{Qch} + R^2{}_{Qdisch}}{5} \quad (8)$$

4.2 Thermal stratification

PTES operation is based on the phenomenon of stratification which occurs due to the difference in densities between two layers of water. Therefore, as cold water has a higher density than hot water, it remains at the bottom part of the storage. A natural barrier called thermocline forms between these water masses, which prevents the cold water from mixing with the hot water. The smaller the area of the thermocline is the better for the whole system because there is less mixing effect which leads to less heat losses and, consequently, means better efficiency of the thermal energy storage. Many stratification indicators have been studied in the literature during these last years but each one of them has limitations depending on the case of study. For example, some stratification indicators are not useful if processes of charging and discharging are being analyzed at the same time or the effect of heat losses are not related with the mixing degree of the storage. Haller et al. (2009) [10] proposed many stratification indicators and efficiencies for different situations of study. In this project, MIX number and stratification coefficient are chosen to evaluate the storage stratification degree. To make it easier and simplified, isovolumetric layers and constant water properties are considered for the calculations of both stratification indicators.

4.2.1 MIX number

This dimensionless number is based on the use of the first moment of energy and has undergone several adaptations. As the most recent one, Andersen et al. (2007) [11] define the MIX number as the difference of moment of energy between a perfectly stratified storage and the experimental storage, to the difference of moment of energy between a perfectly stratified storage and a fully mixed storage. It is necessary to know the definition of the moment of energy concept which is mentioned as “the integration of the sensible energy content along its vertical axis, weighted with the height of its location” (Haller et al., 2009 [10]). The height of each layer corresponds to the height from the bottom to the volumetric center of the layer, which is the middle point of itself. For a better understanding, both moment of energy *(9)* and MIX number *(10)* expressions are presented below:

$$M_E = \sum_{i=1}^{n} y_i \cdot \rho \cdot V_i \cdot C_p \cdot T_i \tag{9}$$

$$MIX = \frac{M_E^{stratified} - M_E^{current}}{M_E^{stratified} - M_E^{fully\ mixed}} \tag{10}$$

The stratification efficiency related with the MIX number *(11)* will take a value of 0 if the storage is fully mixed and will take a value of 1 if it is perfectly stratified, i.e., no mixing between hot and cold water. It can be concluded that the closer the efficiency to 1 the better is the storage stratification degree.

$$\eta_{MIX} = 1 - MIX \tag{11}$$

It has to be pointed out that the MIX number has a limitation related with the complexity of its calculation depending on the storage discretization and the amount of parameters that it depends on.

4.2.2 Stratification coefficient

This indicator was first introduced by Wu and Bannerot (1987) [12] and it is based on the mean square deviation of the storage temperatures from the average temperature. It has to be stated that each layer is weighted with its mass to total mass of the storage but the weight of each layer will be the same because of the considerations already mentioned of isovolumetric layers and constant water properties. The stratification coefficient is calculated as follows *(12)*:

$$S_t = \sum_{i=1}^{n} \frac{m_i \cdot (T_i - T_{av})^2}{m_{total}} \tag{12}$$

4.3 Storage efficiency and capacity

In this project, storage efficiency and thermal capacity are analyzed in order to evaluate the performance of the PTES. As described in section 3.1, considering the storage as a control volume, we can generally define an efficiency as the ratio between the useful output and the input. The storage internal energy change can be taken into account or not, depending on the project considerations. Nevertheless, in this case the internal energy change is considered and therefore the storage efficiency is described on equation *(13)*. The capacity indicator *(14)* refers to the thermal capacity of the storage based on the maximum and minimum temperatures reached during the simulation.

$$\eta = \frac{Q_{disch} + \Delta Q_{storage}}{Q_{ch}} = 1 - \frac{Q_{losses}}{Q_{ch}} \tag{13}$$

$$Capacity = \rho_w \cdot Cp_w \cdot V_{storage} \cdot (T_{max} - T_{min}) \tag{14}$$

5. Description of the TRNSYS model

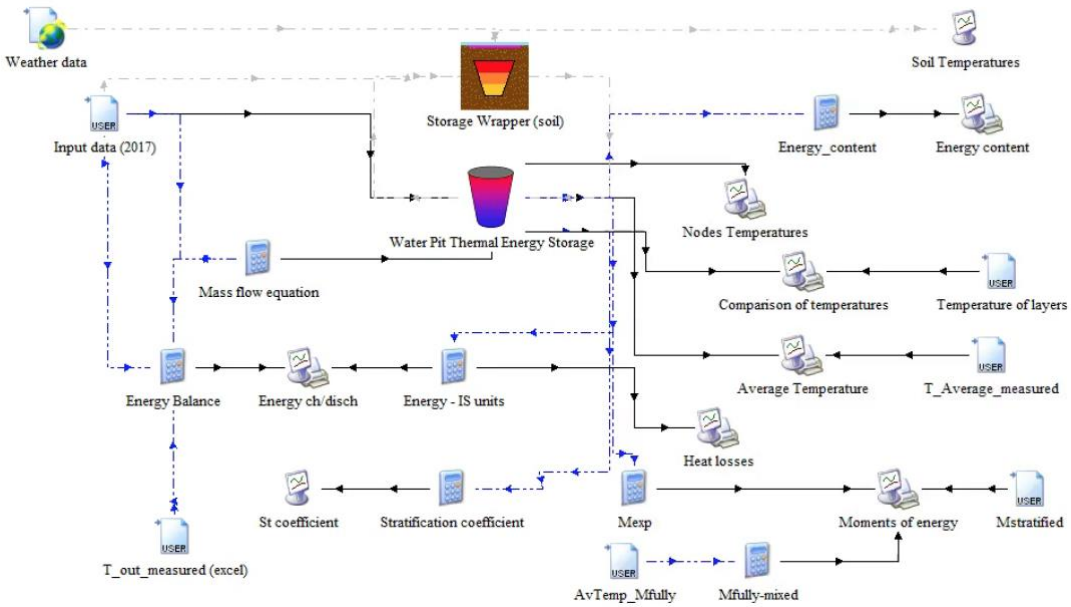

Figure 5. TRNSYS model

In this project, the object of study is a model with a shape of an inverted truncated cone. There are two main components: the first, called “Type 1535”, is used to model the water storage behavior, while the second, called “Type 1301”, is used to model the surrounding soil. Both models have been developed by TESS. Type 1535 is a 1D model because the nodes generation inside the storage is performed along the vertical axis and all calculations are carried out along this axis. On the other hand, type 1301 is a 2D model that generates a mesh along the radial and the vertical axis in order to perform all calculations in both directions. The other secondary elements correspond to data readers, internal calculations to obtain certain useful results and plotters and printers of the final results. Figure 5 presents the complete TRNSYS model with all the links between its components.

5.1 Initial considerations

Before digging deep into the explanation of both main elements of the model, some considerations have been taken into account and are listed below:

- By default, type 1535 allows to use 5 ports as a maximum. A modification on the proforma of the element has been made, changing the maximum number of ports up to 10 since the previous limit of number of ports was not enough for this project development.

- Both the properties of the water inside the storage and those of the surrounding soil are considered constant throughout the project. This is because both type 1535 and 1301 are programmed that way, without taking into account the effect of temperature on all these properties.

- In order to match the models as closely as possible with the actual PTES, at least the volume of the tank, its height and the top surface are kept constant throughout the study.

- In reality, there are sand embankments that were left there once the hole was drilled for the construction of the water pit heat storage. In the model, these embankments are not considered, thus the tank is completely buried and the only part of the storage that is in contact with the environment is the top cover.

- The heat transfer coefficients of top, edges and bottom surfaces are also considered constant during the simulations. Since they are calculated as a function of the convection coefficient of the water on each surface and these are calculated based on average temperatures, all values can be considered acceptable.

- While the thickness of the top insulation is taken into account, the thickness of the HDPE and geotextile liners are disregarded due to their low value. However, their values are used to calculate the thermal resistance for the heat transfer coefficients calculations.

- Mixing inversion inside the storage is not allowed in this project. This means that a node cannot remain colder than the node below it, since this may cause temperatures instabilities in the program.

- Type 1535 allows to consider an immersed heat exchanger inside the storage in order to see the effects that it produces to the PTES performance. In this project, a HX is not taken into account but it may be interesting to consider it in further studies. There is also the option of considering miscellaneous heat flows that may act on the tank but, as there is insufficient data on whether consider them or not, at the end they are not used in this project.

5.2 Parameters and inputs of type 1535

The first parameter is the number of nodes in which the tank is divided, i.e. the discretization. This parameter not only generates a discretization inside the storage but also is responsible of the number of soil cells that are generated in the area that is closest to the sidewall. Another important parameter is the number of ports from where the water goes in and out. The real PTES has three diffusers as explained before and they all work simultaneously in order to keep a good performance of the storage, which means that there is more than one inlet or outlet depending on the operation desired. TRNSYS does not accept more than one inlet or outlet per port, so a modification has been made. This modification consists on considering six ports instead of three because the combination of operation of all six ports ends up being as it would be three ports working. The description of the six ports and the six possible combinations of different operation situations are described on Table 1 and Table 2, respectively.

Number of port	Inlet diffuser	Outlet diffuser
1	Top	Middle
2	Top	Bottom
3	Middle	Top
4	Middle	Bottom
5	Bottom	Top
6	Bottom	Middle

Table 1. Ports composition

Operation	Top diffuser	Middle diffuser	Bottom diffuser	Ports
1	1	1	0	5 & 6
2	1	0	0	3 & 5
3	0	1	1	1 & 2
4	0	0	1	2 & 4
5	0	1	0	1 & 6
6	1	0	1	3 & 4

Table 2. Different operation situations

The indicator of each diffuser means the direction of the water flow, which 0 means inlet flow and 1 means outlet flow. The location of the diffusers is also needed and their position is set to the nodal positions corresponding to the real height of 15.5, 11.2 and 0.5 m. The position of the middle diffuser is set such as that half of the water volume is above it and the other half is below it, so it has the same heat capacity in both regions (Gauthier, 2020 [5]).

The following parameters are related with the geometry of the storage and the water properties. Geometry parameters are basically three: the volume of the storage, which is set to 60000 m^3, the tank height, which is set to 16 m and the ratio of tank radii, which is the ratio between the top radius and the bottom radius. Only the last geometry parameter is the variable one since the other two are considered constant as it was mentioned on the considerations of the project. Water properties are also considered constant and independent of the temperature because it is how is established. According to Bergman et al. (2011) [13], water properties can be set as follows:

Property	Symbol	Value	Units
Specific heat	C_p	4.19	kJ/(kg·K)
Density	ρ	1000	kg/m^3
Thermal conductivity	λ	0.6	W/(m·K)
Dynamic viscosity	μ	$8.92 \cdot 10^{-4}$	kg/(m·s)
Thermal expansion coefficient	β	$2.6 \cdot 10^{-4}$	1/K

Table 3. Water properties used in type 1535

For the initial node temperatures there are two methods to get them. One method is to take advantage of the model calibration and take the final values from 2016 as the initial values of 2017 or use directly the initial values from the experimental data. If the second method is chosen it has to be taken into account that depending on the discretization of the storage, i.e, the number of nodes, a regression is needed to obtain precise values. With the temperatures of the 32 experimental layers, a regression is made with the temperature on function of the position of the layer within the storage. Then, this regression equation can be applied with other number of nodes and obtain the corresponding initial temperatures with the new storage discretization.

The last parameters are the heat transfer coefficients of top, sides and bottom of the storage. The value of the top heat transfer coefficient is based on the thermal resistance of outdoor surfaces presented by Ochs in 2009 [14], which is established as 25 W/(m^2·K). It has to be taken into account the degradation of the insulation thermal conductivity due to moisture and high temperatures. That is why a higher value of 26.6 W/(m^2·K) of the heat transfer coefficient between the top part of the storage and the insulation is chosen based on studies that worked with similar models (Xie et al., 2021 [6]). There is another method to guess the heat transfer coefficient of the cover based on convection and radiation effects. The problem is that it is an iterative method and the convection and radiation coefficients also have to be

calculated and they depend on more variables. In the end, the value of 26.6 W/(m^2·K) is considered correct for use in this project.

Since there is no insulation between the sides and the bottom part of the PTES, the heat transfer coefficient is based on water convection and thermal conduction through the HDPE liner and the geotextile layer. Observing the operation of the PTES, it can be said that the impact of water natural convection is much higher than the forced convection caused by the inlet and outlet of water flow. Comparing the charging and discharging operation modes with the situation in which the storage is on standby, the last situation has more weight (Gauthier, 2020 [5]). Both heat transfer coefficients from the side and the bottom are obtained from *(15)* and *(16)*, where a factor is added to compensate the surface difference between the real storage and the model.

$$U = f_{area} \cdot \frac{1}{\frac{1}{h_w} + \frac{\delta_{HDPE}}{\lambda_{HDPE}} + \frac{\delta_{geo}}{\lambda_{geo}}} \tag{15}$$

$$f_{area} = \frac{A_{real}}{A_{model}} \tag{16}$$

The natural convection coefficient can be calculated by equations *(17)*, *(18)*, *(19)* and *(20)* (Bergman et al., 2011 [13]). The first two equations are to calculate the natural convection coefficient of an inclined wall and the last two are to calculate the natural convection coefficient of a cold plate, which can be geometrically similar to the bottom surface of the storage. All the water properties that are dependent of temperature are calculated considering the real annual average temperature of both side and bottom, which are 35 ºC and 25 ºC respectively. The difference of temperature between the inner and outer cell is assumed to be 10 ºC (Forkel and Daniels, 1995 [15]).

$$h_{side} = \frac{\lambda_{w,side} \cdot \sin(\theta)}{H} \left\{ 0.825 + \frac{0.387 \cdot (Gr_{w,side} \cdot Pr_{w,side})^{\frac{1}{6}}}{\left(1 + \left(\frac{0.492}{Pr_{w,side}}\right)^{\frac{9}{16}}\right)^{\frac{8}{27}}} \right\}^2 \tag{17}$$

$$Gr_{w,side} = \frac{\cos(\theta) \cdot g \cdot \beta_{w,side} \cdot (T_{side} - T_w) \cdot H^3}{{\upsilon_{w,side}}^2 \cdot sin(\theta)^3} \tag{18}$$

$$h_{bot} = \frac{0.6 \cdot \lambda_{w,bot}}{H} \cdot \left(Gr_{w,bot} \cdot Pr_{w,bot}\right)^{\frac{1}{3}} \quad (19)$$

$$Gr_{w,bot} = \frac{g \cdot \beta_{w,side} \cdot (T_{bot} - T_w) \cdot {D_{bot}}^3}{64 \cdot {\upsilon_{w,bot}}^2} \quad (20)$$

To introduce the inputs to the storage, an element offered by TRNSYS is used, which consist of a data reader. Using MATLAB, an input file is created by extracting from the measurement data all the inlet temperatures, flows and ambient temperatures for each timestep. This file is developed in such a way that at each timestep the inlet flow considered is the highest at that time since it is assumed to be equal between the inlet and outlet.

The last input is the loss temperature for each storage node. These temperatures are an output of type 1301 and are the ones that are used to calculate heat losses from the storage. The obtention of their values is explained on the following section since the other element is in charge of calculating them.

5.3 Parameters and inputs of type 1301

The soil surrounding type shares the geometrical parameters with type 1535 such as the storage volume, the height and the ratio of tank radii. The parameters related with the top insulation are set in this element, which are the insulation thickness of 0.24 m and its thermal resistance of 6 (m^2·K)/W, which is described on equation *(21)*.

$$R_{ins} = \frac{\delta_{ins}}{\lambda_{ins}} \quad (21)$$

The geological study (PlanEnergi, 2011 [8]) of the surrounding soil and a reported paper about properties of different kind of sand (Hamdhan et al., 2010 [16]) are useful to choose the soil properties. In this project a thermal conductivity of 0.4 W/(m·K), density of 2000 kg/m^3 and a specific heat of 0.84 kJ/(kg·K) are used as soil properties.

This type permits to choose different ways to calculate the heat transfer to the soil surface, both insulated and uninsulated sections. In this project, equations *(22)* and *(23)* are used to set the temperature of the soil surface as a function of the soil properties (α_{soil}), depth

(z) and the time of the year (t) (Kusuda et al., 1965 [17]). T_s is the mean surface temperature based on the annual average air temperature of the location in question and it is set to 9 ºC (Climate Data, [18]). ΔT_s is the amplitude of the surface temperature of undisturbed soil over the course of a year and its value is decided to be 5 ºC. The parameter θ corresponds to the day of the minimum surface temperature, which is established as the 53th day of the year, i.e., the 22nd of February (Climate Data, [18])

$$T(z,t) = \overline{T_s} - \Delta\overline{T_s} \cdot e^{-z*\sqrt{\frac{\pi}{\alpha_{soil}\cdot 365}}} \cdot \cos\left(\frac{2\pi}{365} * \left(t - \theta - \frac{z}{2} * \sqrt{\frac{365}{\alpha_{soil}\cdot\pi}}\right)\right) \quad (22)$$

$$\alpha_{soil} = \frac{\lambda_{soil}}{\rho_{soil}\cdot Cp_{soil}} \cdot 24 \quad \left[\frac{m^2}{day}\right] \quad (23)$$

Other parameters that are needed for the generation of the grid meshing are the far-field and deep earth distance, which are the horizontal distance from the edge of the insulation and the vertical distance from the bottom surface of the tank at which the soil is assumed to be unaffected by the heat transfer of the tank. The far-field distance is set to 200 m which is more or less two times the top diameter of the storage and the deep earth distance is set to 40 m.

The size of the smallest nodes, which are the closest to the surrounding of the tank and therefore the most affected by the temperature gradient, is established as 0.05 m. The smaller the size the more accurate the results, but the calculation time that is needed is higher. There is also a scalar used to size adjacent soil nodes as they move outwards away from edges. This multiplier has been set to 2.

The inputs that type 1301 needs are the temperature of nodes that are calculated by type 1535, weather data from a weather data reader supplied by TRNSYS, the ambient temperature from the input file and the heat transfer coefficients explained on the previous section.

6. Storage and soil temperatures

6.1 Storage temperatures and heat transfer

For the storage temperature calculations, vertical thermal conduction, forced convection due to charging and discharging operations and heat transfer between the storage and the soil are taken into account. The calculation is based on a differential equation *(24)* which describe the evolution of the storage temperatures as a function of the capacitance and all the phenomena described previously. Equations *(25)*, *(26)* and *(27)* describe the elements that compound the differential equation. Parameters A and B are defined as the exported heat coefficient from the node (W/K) and the imported heat into the node (W), respectively. Parameter B has two possible expressions depending on whether the node in question corresponds to an input node or not, since the layer heat transfer is directly affected for the inlet flow. T_{loss} refers to the adjacent soil node temperature, which is calculated according to equation *(22)* explained in section 5.3. The contact surface between the storage nodes and the soil nodes is described in *(28)*, where Δz_j is the vertical length of each node and r_j is the radial distance from the symmetry axis to the center of the node.

$$V_j \cdot Cp \cdot \rho \cdot \frac{\partial T_j}{\partial \tau} = A * T_j + B \tag{24}$$

Where:

$$A = \left(-K_j - \dot{m}Cp\right) - \left(K_{j-1} + \dot{m}Cp\right) - U_j A_j \tag{25}$$

Inlet flow

$$B = \left(K_j + \dot{m}Cp\right) \cdot Tav_{j+1} + \left(K_{j-1} + \dot{m}Cp\right) \cdot Tav_{j-1} + U_j A_j \cdot T_{loss} + \dot{m}Cp \cdot T_{in} \tag{26}$$

Without inlet flow

$$B = \left(K_j + \dot{m}Cp\right) \cdot Tav_{j+1} + \left(K_{j-1} + \dot{m}Cp\right) \cdot Tav_{j-1} + U_j A_j \cdot T_{loss} \tag{27}$$

$$A_{side} = \pi \cdot \left(r_j + r_{j-1}\right) \cdot \sqrt{{\Delta z_j}^2 + \left(r_j - r_{j-1}\right)^2} \tag{28}$$

Within the source code of this type, is used a subroutine related with the geometrical parameters needed to characterize each node inside the storage. This parameters include the volume, the top, edge and bottom surfaces, the conduction area and length of each node. The heat transferability due to vertical thermal conduction can be calculated as *(29)*. Even though this would be more adequate for a node that has a constant perpendicular area along the vertical axis, the calculation is considered correct.

$$K_j = \frac{\pi \cdot {D_j}^2}{4} \cdot \frac{\lambda_w}{L_{cond}} \tag{29}$$

6.2 Soil temperatures and heat transfer

As mentioned on the introduction of section 5, the nodal grid generated within the element that simulates the soil is in 2D. In other studies that use another element with a similar shape as the one in this case, they present a precise description of the 2D grid. In this project, the description of the generated grid will not be so precise due to a lack of information of how some subroutines of the source code generate some parts of the mesh. A really good guessing can be made because the source code provides enough information to do it.

First of all the nodes are generated along the vertical axis. In this group it can be distinguished the ones that belong to the insulation above the top of the tank, the ones that belong to the storage itself and finally the ones that go from the bottom part of the storage until the deep earth boundary. The only difference between these nodes are the vertical size of them. While the ones that are part from the insulation and the storage have the insulation thickness and layer height as a vertical size, the rest of the nodes increase their vertical size according to the scalar value established on the parameters.

The next step is the nodal generation along the radial axis. The firsts generated are the ones that are distributed from the origin of coordinates until the bottom radius. They are generated from bigger to smaller size again according to the scalar value. This kind of nodal generation means that the densest nodes are the closest to the bottom corner. From the bottom radius to the insulation edge, nodes have the same increasing value along the radial axis even though its total size is not the same. In the end, last nodes that are generated are the ones that have the limit when the far-field boundary is reached.

Type 1301 classifies the nodes that constitute the grid meshing into three big groups in order to calculate the heat transfer on both directions of each node as a function of its position within the mesh. The first group is formed by the nodes that belong to the storage and, besides considering vertical thermal conduction between them, heat transfer between the storage and the insulation and the soil is also considered. The second group is formed by the nodes that are generated closest to the slope. There are as many nodes along the sidewall as layers inside the storage. These are the nodes that exchange heat with the nodes inside the storage and also with its neighboring soil nodes in both directions. The last big group is formed by the rest of the nodes, both those who are distributed from the tank's bottom to the deep

earth boundary and those who are distributed from the edge of the insulation until the far-field boundary. It has to be said that the nodes that are in the region between the bottom corner and the edge of the insulation and in addition they are not the closest to the sidewall form part of this last big group as well.

For a better comprehension, Figure 6 depicts a grid meshing similar to the one generated in this project but with the difference that in this project twice as many nodes are formed close to the inclined wall. The mesh of the figure belongs to the study conducted on type 343 (Xie et al., 2021 [6]).

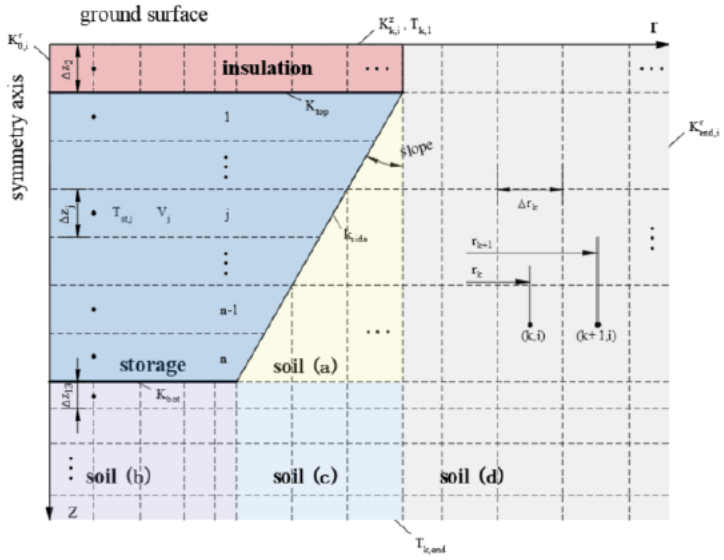

Figure 6. Description of type 343 grid meshing

Type 1301 also uses a differential equation *(30)* to calculate the evolution of temperatures based on the capacitance of each node and heat transfer between nodes. Its components are described on equations *(31)* and *(32)*.

$$Cap_{r,z} \cdot \frac{\partial T_{r,z}}{\partial \tau} = A \cdot T_{r,z} + B \tag{30}$$

Where:

$$A = -K^r_{i,z} - K^r_{i-1,z} - K^z_{r,i} - K^z_{r,i-1} \tag{31}$$

$$B = K^r_{i,z} \cdot Tav_{i,z} + K^r_{i-1,z} \cdot Tav_{i-1,z} + K^z_{r,i} \cdot Tav_{r,i} + K^z_{r,i-1} \cdot Tav_{r,i-1} \tag{32}$$

The capacitance of each node depends on soil properties and geometrical parameters. The expressions *(33)* and *(34)* define the capacitance and conduction surface, where Δz_z and Δr_r are the horizontal and vertical lengths of each node and r_r is the radial distance from the symmetry axis to the center of the node.

$$Cap_{r,z} = A_{r,z} \cdot \Delta z_z \cdot \rho_{soil} \cdot Cp_{soil} \tag{33}$$

$$A_{r,z} = \pi \left(\left(r_r + \frac{\Delta r_r}{2} \right)^2 - \left(r_r - \frac{\Delta r_r}{2} \right)^2 \right) \tag{34}$$

Soil nodes heat transfer depends on its position and the direction of the heat flow. The heat transferability can be summarized by equations *(35)*, *(36)*, *(37)* and *(38)*, depending on the region where the heat transferability takes place, i.e., soil region or insulation layer.

$$K_{i,z}^{r} = \left(\frac{log\left(\frac{r_{i+1}}{r_i}\right)}{2 \cdot \Delta z_z \cdot \lambda_{soil}} \right)^{-1} \tag{35}$$

$$K_{r,i}^{z} = \left(\frac{\Delta z_i + \Delta z_{i+1}}{2 \cdot \lambda_{soil} \cdot A_{r,z}} \right)^{-1} \tag{36}$$

$$K_{i,z}^{r} = \left(\frac{log\left(\frac{r_{i+1}}{r_i}\right)}{2 \cdot \Delta z_z \cdot \lambda_{ins}} \right)^{-1} \tag{37}$$

$$K_{r,i}^{z} = \left(\frac{\Delta z_i + \Delta z_{i+1}}{2 \cdot \lambda_{ins} \cdot A_{r,z}} \right)^{-1} \tag{38}$$

There are some special cases within the previous equations depending on the nodes surroundings. The vertical heat transfer between the nodes located just below the bottom of the storage and the ones that are located inside the tank is described by *(39)*, as it has to be taken into account two thermal resistances. There is also another special case related with the heat transfer between the insulation and the soil, which is referred on *(40)*.

$$K_{r,i}^{z} = \left(\frac{\Delta z_i}{2 \cdot \lambda_{soil} \cdot A_{r,z}} + \frac{1}{U_{bot} \cdot A_{r,z}} \right)^{-1} \tag{39}$$

$$K_{i,z}^{r} = \left(\frac{log\left(\frac{r_i + \frac{\Delta r_i}{2}}{r_i}\right)}{2 \cdot \Delta z_z \cdot \lambda_{ins}} + \frac{log\left(\frac{r_{i+1}}{r_i + \frac{\Delta r_i}{2}}\right)}{2 \cdot \Delta z_z \cdot \lambda_{soil}} \right)^{-1} \quad (40)$$

The nodes that are closer to the sidewall are not only affected by the soil heat transfer but also for the heat transfer with the storage. Therefore, the A *(42)* and B *(43)* factors from the differential equation *(41)* are a little bit different. One more thing to note is the fact that only half of the soil capacitance is considered on this nodes since the other half of the capacitance correspond to the storage adjacent nodes.

$$\frac{Cap_{r,z}}{2} \cdot \frac{\partial T_{r,z}}{\partial \tau} = A' \cdot T_{r,z} + B' \quad (41)$$

$$A' = -K_{i,z}^{r} - K_{r,i}^{z} - U_{side} A_{side} \quad (42)$$

$$B' = K_{i,z}^{r} \cdot Tav_{i,z} + K_{r,i}^{z} \cdot Tav_{r,i} + U_{side} A_{side} \cdot T_{loss} \quad (43)$$

7. Basis Model - Model 1

The storage of the first model is discretized with 20 layers. It is the basis model because all the following models are created from this, either trying to improve its final values or changing other parameters to see their influence on the final results. As mentioned in section 5.1, storage volume and tank height are the only parameters that will be constant in all the analyzed models during this project. To keep the slope of 26.6º and the top surface equal to the one from the actual PTES, the model bottom surface suffers a slight dimension change due to geometry, since the model has a shape of an inverted truncated cone and the real storage has a shape of an inverted truncated pyramid. Equations *(44)*, *(45)* and *(46)* refer to the geometrical equations from both model and real storage which are used to calculate the top and bottom radius and therefore the ratio of tank radii. The location of the top, middle and bottom diffusers are set to layers 1, 6 and 20 respectively, according to the real diffusers positions. Table 4 shows all the geometrical parameters of Model 1 and Table 5 shows the parameters that directly or indirectly depend on the geometrical ones, i.e. the convection coefficients of the sidewall and bottom and consequently the heat transfer coefficients.

$$A_{top,real} = {L_{top,real}}^2 \tag{44}$$

$$A_{top,model} = \pi \cdot {R_{top,model}}^2 \tag{45}$$

$$V_{model} = \frac{\pi \cdot h}{3} \cdot \left({R_{top}}^2 + {R_{bot}}^2 + R_{top} \cdot R_{bot}\right) \tag{46}$$

$A_{top,real}$ [m²]	$A_{top,model}$ [m²]	V [m³]	Slope [º]	h [m]	R_{top} [m]	R_{bot} [m]
8100	8100	60000	26.6	16	50.78	15.20

Table 4. Geometrical parameters of Model 1

Parameter	Bottom	Side
f_{area}	0.93	1.03
h [W/(m²·K)]	400	335
δ_{HDPE} [m]	$2.5 \cdot 10^{-3}$	$2.5 \cdot 10^{-3}$
λ_{HDPE} [W/(m·K)]	0.44	0.44
δ_{geo} [m]	$1 \cdot 10^{-3}$	$1 \cdot 10^{-3}$
λ_{geo} [W/(m·K)]	0.45	0.45
U [W/(m²·K)]	89.40	94.53

Table 5. Parameters for the Model 1 bottom and sidewall heat transfer coefficients calculation

The differences between the real data and the results after the Model 1 simulation are listed on Table 6. The key parameters are the annual charge and discharged energy, internal energy change of the storage, thermal capacity, storage efficiency and heat losses.

Parameter	Measurement data	Model 1
Charged energy [MWh]	11868	11779
Discharged energy [MWh]	11250	11404
Internal energy change [MWh]	-539	-500
Maximum temperature [ºC]	84.4	85.5
Minimum temperature [ºC]	8.7	8.6
Thermal capacity [MWh]	5286	5365
Storage efficiency (%)	90	93
Total heat losses [MWh]	1157	853
Top heat losses [MWh]	580	552
Edge heat losses [MWh]	-	286
Bottom heat losses [MWh]	-	15

Table 6. Key parameters from Model 1

The annual charged and discharged energy in the model have a different behavior according to its value. While the annual charged energy has a lower value than the real one, the discharged energy is higher than its corresponding value. The reason why this phenomena occurs can rely on the big error that appears on the discharging operation condition from the port that involves the middle and bottom diffuser. More specifically, this happens when the water is leaving the storage through the middle diffuser and getting into the storage through the bottom. As it can be seen on Table 7, where the charged and discharged energy is classified according to the operation condition, the deviation between the experimental data and the model is -81%. This can seem a very high deviation but it is finally accepted because the discharged energy in that operation condition is low compared with the other operation conditions that involves the rest of the diffusers. The deviation among the total annual charged and discharged energy and the thermal capacity is around -1% so these can be considered as very accurate results. The 24% of difference between real heat losses and the simulated ones can rely on the difference that can also be seen from the internal energy change, which has a deviation of 7%. Since the values of charged and discharged energy are pretty accurate, it can be supposed that the difference on heat losses are not caused by them.

Using TRNSYS, diffusers outlet temperatures can be compared with the temperatures corresponding to the experimental layers named on the introduction of this section. Figure 7 and Figure 9 show the results where top and bottom temperatures match pretty well with the

measurement data. The mismatch of the middle diffuser starts when the general operating condition switches from discharge to charge, as it can be observed on Figure 8.

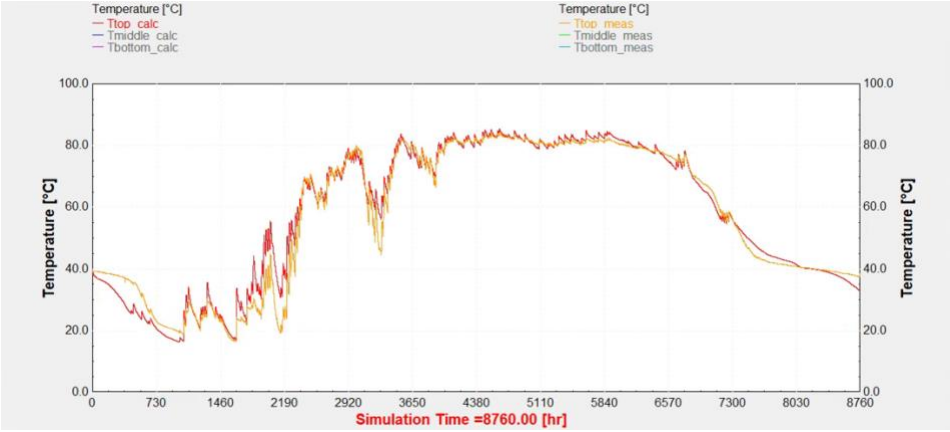

Figure 7. Comparison of the evolution of top diffuser outlet temperature from Model 1

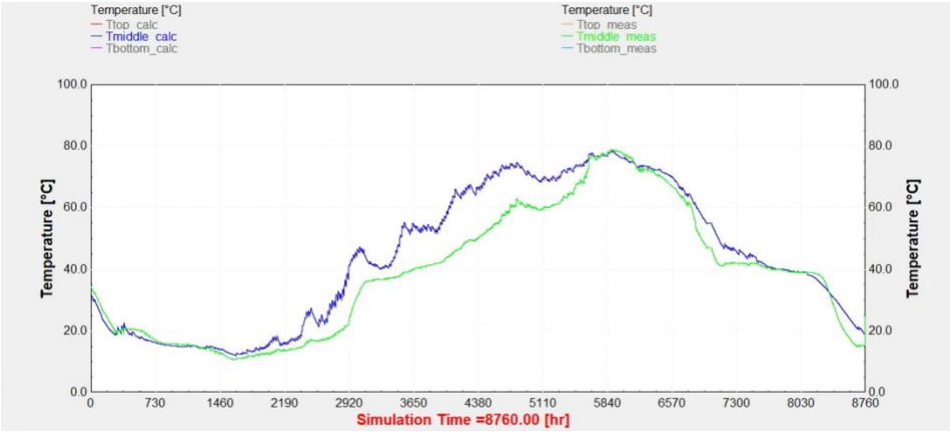

Figure 8. Comparison of the evolution of middle diffuser outlet temperature from Model 1

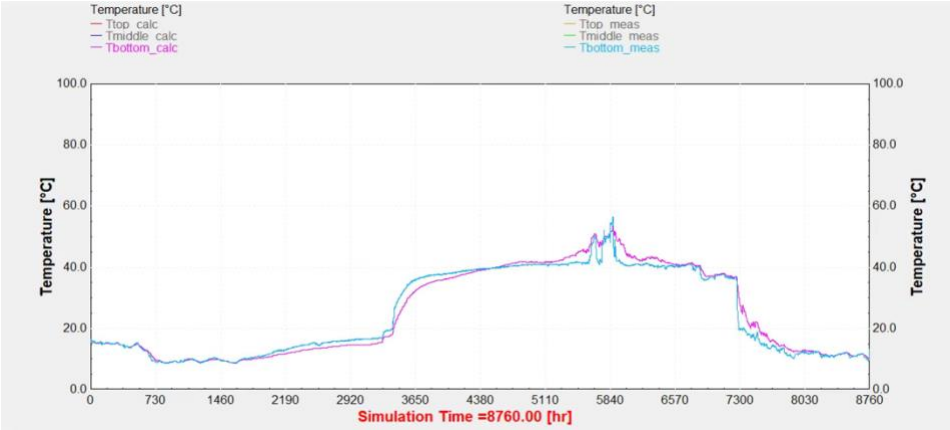

Figure 9. Comparison of the evolution of bottom diffuser outlet temperature from Model 1

The average storage temperature is presented in Figure 10 and also has a mismatch with the volume-weighted average measured temperature. This process of weighting each layer according to its volume with respect to the total is necessary to compare as accurately as possible two models that are discretized in such a different way. The error also appears when the general operation condition switches from discharge to charge, which suggests that the reason for this is the same that produces the mismatch of the middle diffuser outlet temperature. In fact, something that should be noted is that when the mismatch is produced, the simulation has higher values than the measurement. The origin of this phenomenon can be due to two possible reasons, either the simulation overestimates the results when it is time to switch the general operation condition or the measurement has some problem related to the data collection within these periods.

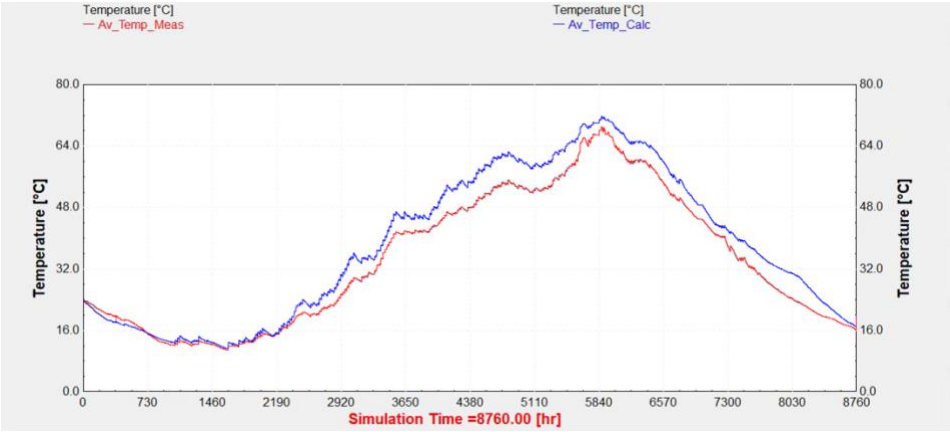

Figure 10. Comparison of the evolution of the average temperature from Model 1

The evolution of the monthly charged and discharged energy is also interesting to analyze because it is very representative of the operation of the water pit heat storage during a whole year. As it can be seen on Figure 11, the period of the year when the energy charged to the storage (energy input) is higher starts in April and ends in August, which describes consistently the seasonal storage behavior. When the temperatures are higher, the solar array can heat the water until higher temperatures, so it is the perfect time to heat the upper part of the water pit to increase its temperature.

When we talk about discharged energy, the results are not that clear as the ones from charged energy. The highest quantity of discharged energy is in October, which is consistent because the demand of heat is high. The amount of discharged energy is pretty regular on the rest of the months except on February, March, April and August. This occurs because this PTES

is not only based on seasonal storage but also there are inputs and outputs based on days and nights just to keep as high as possible the thermal stratification of the storage. In further studies maybe it would be interesting to analyze the charged and discharged energy not only monthly but also between day and night, even though the amount of data to treat would be too big.

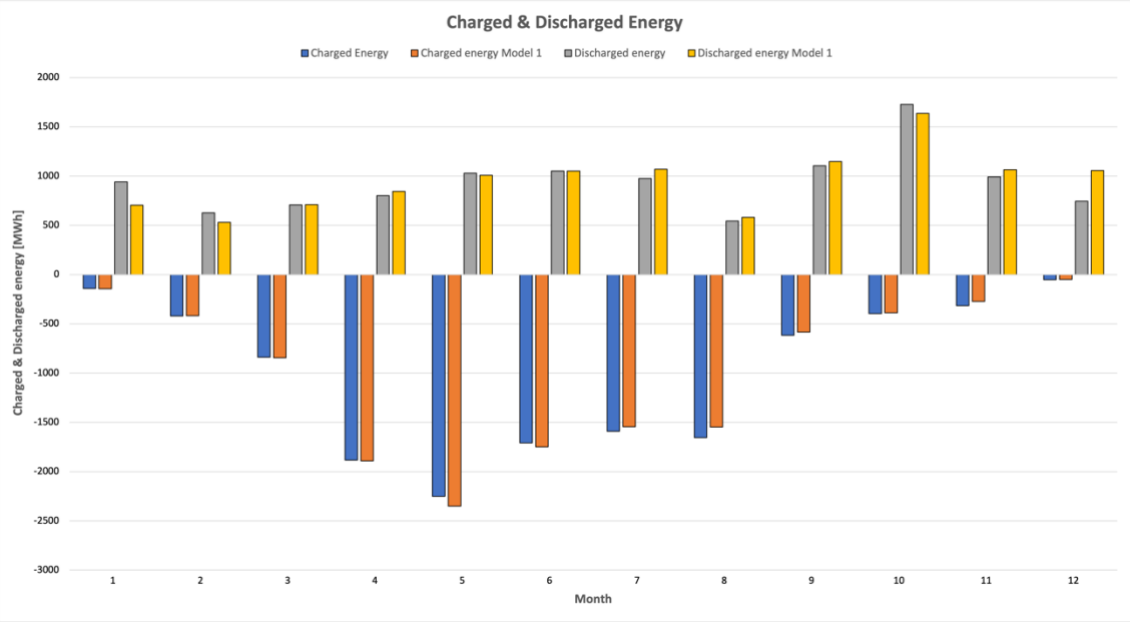

Figure 11. Comparison of monthly charged and discharged energy from Model 1

A studio has also been carried out between different ports to see the influence that every port has in terms of charged and discharged energy (Table 7). We can find the most clarifying behavior between the top and bottom diffusers. As we can see on the results, when it is charging energy time, the hot water gets into the storage through the top diffuser and the cold water leaves the tank through the bottom one. It also happens the same phenomenon but inverted when it is discharging time. When both diffusers work at the same time, the charged energy represents around 80% of the total and the discharged energy between the 78% and 83% of the total.

When the middle diffuser is involved in the PTES operation, the behavior of the water pit is not as clear as the previous situation. One can think that the hot water always has to get into the storage through the top diffuser but sometimes the water that comes from the solar array is not hot enough and therefore, to keep the thermal stratification of the storage, the water flow goes in through the middle diffuser. The same applies to the cold water inlet or outlet. The amount of charged energy when the top and middle diffuser work simultaneously

represents between the 7% and 8% of the total charged energy while the discharged energy represents around the 10% of the total discharged energy.

Condition	Top – Bottom	Top – Middle	Middle - Bottom
Charge			
Measurement [MWh]	9565	973	1584
Model 1 [MWh]	9644	864	1527
Error (%)	-1	11	4
Discharge			
Measurement [MWh]	9431	1181	891
Model 1 [MWh]	8897	1147	1615
Error (%)	6	3	-81

Table 7. Values of charged and discharged energy according to different ports from Model 1

The evolution during the year and the monthly total values of heat losses are showed on Figure 12 and Table 8. In this case, a negative value of heat losses means heat gain from the storage, which means the heat transfer on that certain area goes towards the inside of the tank instead towards the soil. This occurs because the global temperature of the surrounding soil is higher than the storage temperature. A relation between the charged and discharged energy and heat losses can be found, therein during the global charging period heat losses are higher due to the temperature increase inside the storage. Losses through the top part of the storage are the ones that have higher values within the total heat losses. Indeed, top heat losses represent around the 65% of the total heat losses, followed by a 33% and 2% of edge and bottom losses respectively.

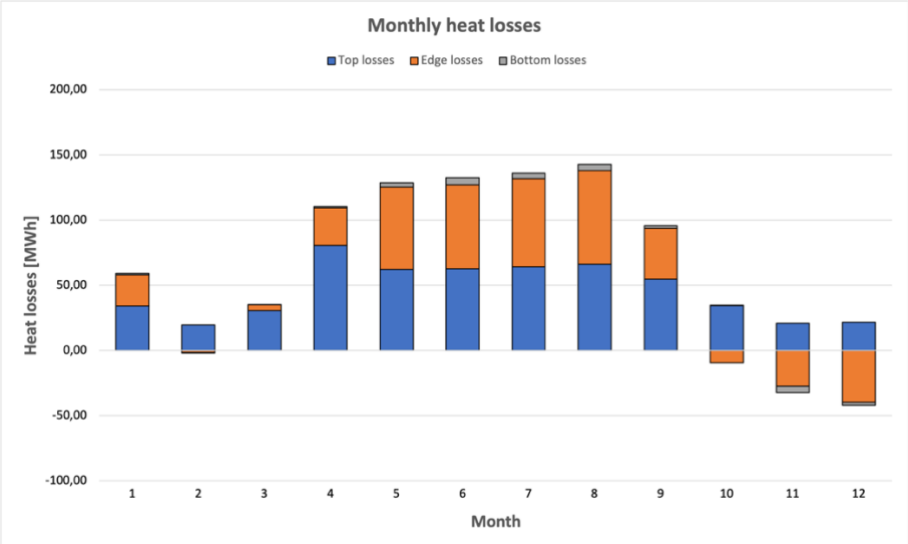

Figure 12. Annual evolution of heat losses from Model 1

Month	1	2	3	4	5	6	7	8	9	10	11	12
Losses [MWh]	59	18	35	111	129	132	136	143	96	26	-11	-20

Table 8. Monthly total heat losses from Model 1

In relation to thermal stratification, the MIX number efficiency (Figure 13) and the stratification coefficient (Figure 14) do not follow a similar evolution pattern according to the PTES operation. It is true that when the change of the operation condition from discharge to charge occurs, both thermal stratification indicators present their maximum value. This means that the storage is efficiently charged due to the correct use of the diffusers. Another aspect to highlight is the fact that during the general discharge period the model is not performing as it should because both values are generally lower than the real data. This inefficient discharge may be due to the fact that the model produces unnecessary discharges of water. In fact, the model globally discharges more energy than the experimental storage, as discussed previously. Another difference that can be observed between both indicators is that when the total charged energy decreases its value within the charge period, the stratification coefficient suffers a drop while the MIX number efficiency remains more or less constant within its low value. Hence, the comment made that both indicators do not follow a very similar pattern as they should since they are used to evaluate the same parameter, i.e., thermal stratification of the storage.

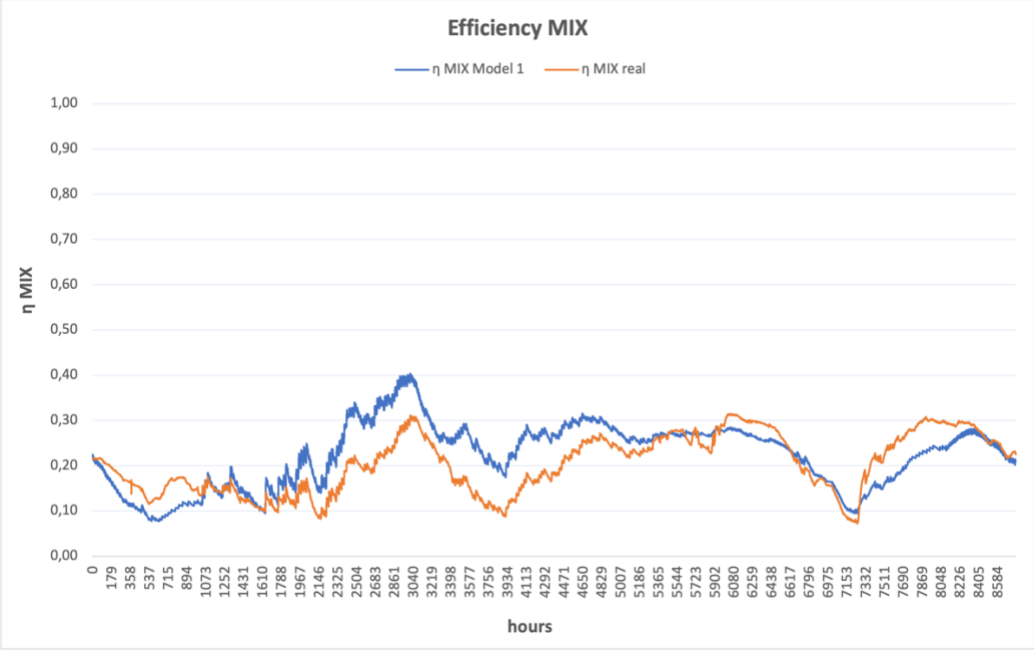

Figure 13. Annual evolution of the MIX number efficiency from Model 1

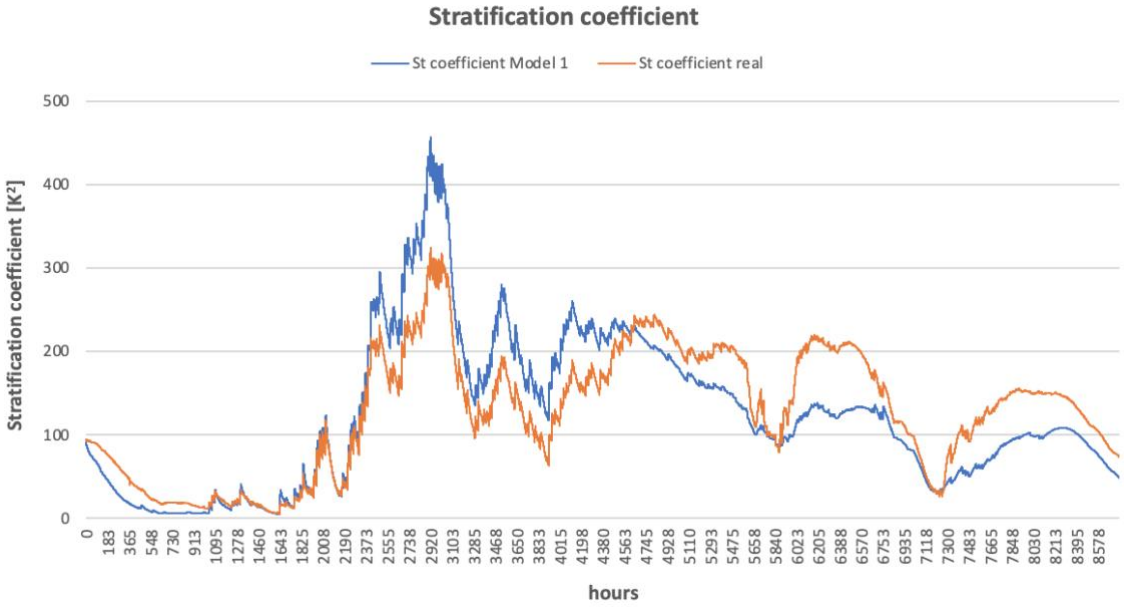

Figure 14. Annual evolution of the stratification coefficient from Model 1

8. Discretization evaluation – Models 2 and 3

The number of layers into which the storage is divided is another object of study since it may influence the results due to the change in size of both the storage nodes and the generated soil nodes that are closer to the sidewall. Model 2 is divided into 32 layers, which is the same distribution in which the temperature sensors are located in the actual storage. The three diffusers are positioned in layers 1, 10 and 32 according to its real position. To create Model 3, the amount of layers is increased to 48 to observe whether the discretization into a large number of nodes has a positive effect on the final results or not. In this model, the three diffusers are positioned in layers 1, 14 and 48. The rest of the parameters and inputs are the same as those used in Model 1. It should be noted that other models with more layers have been considered to study, but type 1301 has been coded in such a way that it has a limitation of 50 nodes. Therefore, the fact that the largest number of layers considered is 48 is enough to see the effects of the model discretization.

Parameter	Measurement data	Model 2	Model 3
Charged energy [MWh]	11868	11997	12038
Discharged energy [MWh]	11250	11598	11644
Internal energy change [MWh]	-539	-485	-477
Maximum temperature [ºC]	84.4	86.3	86.2
Minimum temperature [ºC]	8.7	8.6	8.6
Thermal capacity [MWh]	5286	5430	5416
Storage efficiency (%)	90	93	93
Total heat losses [MWh]	1157	861	853
Top heat losses [MWh]	580	562	568
Edge heat losses [MWh]	-	284	278
Bottom heat losses [MWh]	-	15	7

Table 9. Key parameters from Model 2 and Model 3

The results from Table 9 display an increase tendency of both charged and discharged energy with an increase of the number of layers in which the storage of the model is divided. The more layers the model has the more decreases the internal energy change value, which means that the storage suffer less changes of the global temperature. Taking both aspects into account, the continuous decreasing of the total heat losses can be justified even though the Model 1 has the same heat losses than Model 3. Both thermal capacities are pretty similar because in both models the maximum and minimum temperatures are the same. In terms of the storage efficiency, no significant changes are appreciated because its value remains constant.

The diffusers outlet temperatures have a similar behavior to Model 1. Top and bottom outlet (Figures 15 and 17) temperatures still show high accuracy with the experimental data while the temperature of the middle diffuser (Figure 16) is overestimated when the general operation condition switches from discharge to charge. The accuracy of all models is going to be precisely analyzed in later sections with the coefficient of determination method since graphically it is difficult to observe any significant difference.

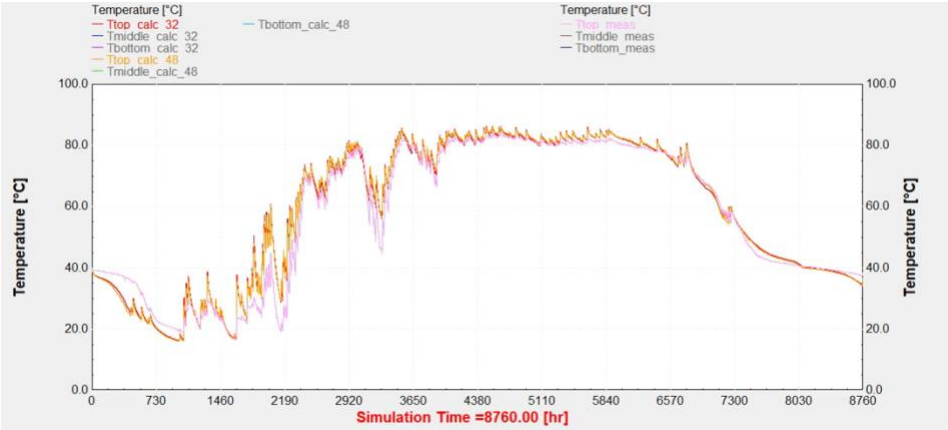

Figure 15. Comparison of the evolution of top diffuser outlet temperature from Models 2 and 3

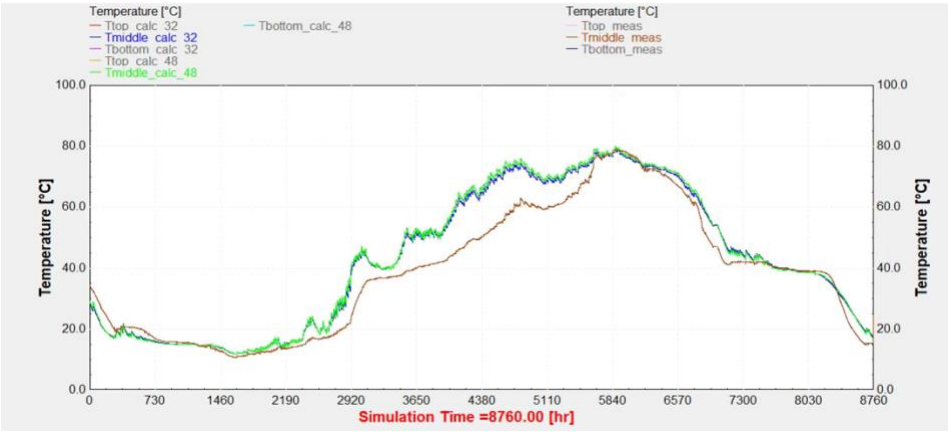

Figure 16. Comparison of the evolution of middle diffuser outlet temperature from Models 2 and 3

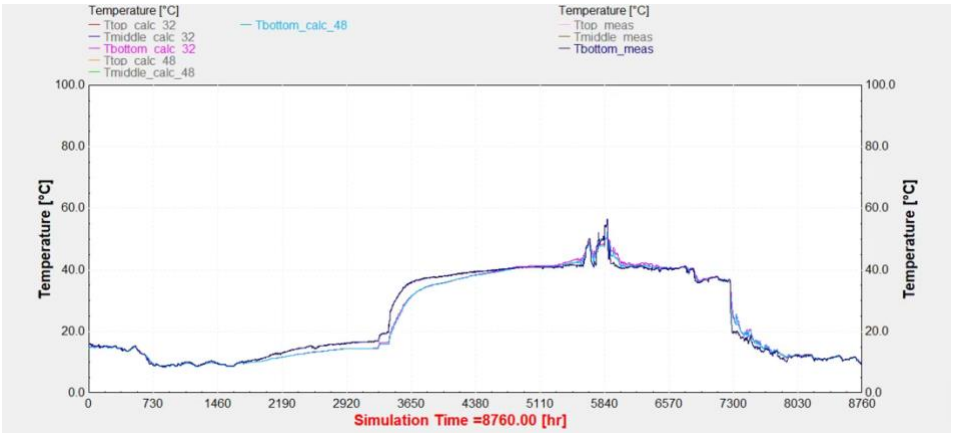

Figure 17. Comparison of the evolution of bottom diffuser outlet temperature from Models 2 and 3

The annual average temperature is more accurate in Models 2 and 3 because the curve is closer to the one from the experimental data, which means the average temperature inside the storage is not as overestimated as in Model 1. In fact, the maximum difference between the model and the actual data decreases from 7.2 °C in Model 2 to 6.6 °C in Model 3. Observing Figure 18 and taking into account this tendency, it seems the accuracy in terms of average temperature is better as more layers has the model.

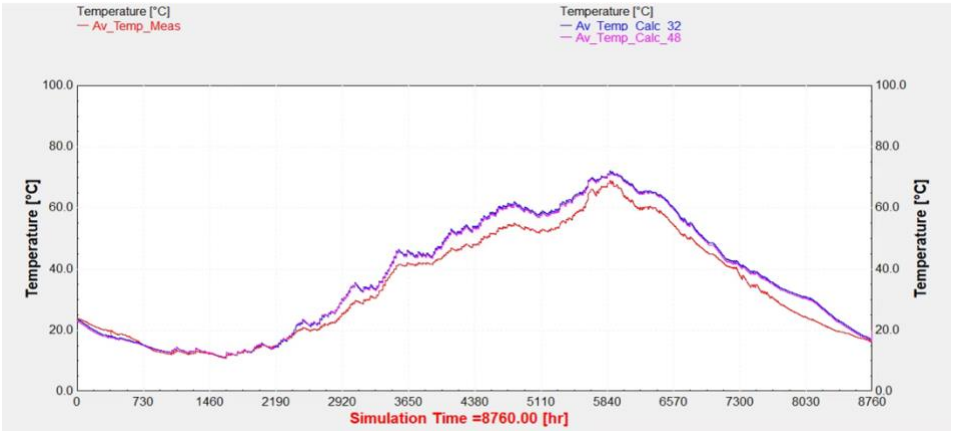

Figure 18. Comparison of the evolution of the average temperature from Models 2 and 3

The evolution of charged and discharged energy is similar to the previous model (Figure 19). In most of the months, charged and discharged energy from Models 2 and 3 is higher than the experimental data. The maximum values of both charged and discharged energy belong to the model that is divided into more layers. This can be appreciated in the total values of the energy delivered since it was mentioned before, the more layers the model has the more energy was transferred inside and outside the PTES. Another aspect to highlight is the fact that whereas the highest value of the charged energy corresponds to a simulated

value, the highest value of the discharged energy corresponds to the actual data. This also happens with Model 1 in the previous section. The biggest deviation of the discharged energy (-310 MWh) takes place in December while the biggest deviation of the charged energy occurs in May (-142 MWh).

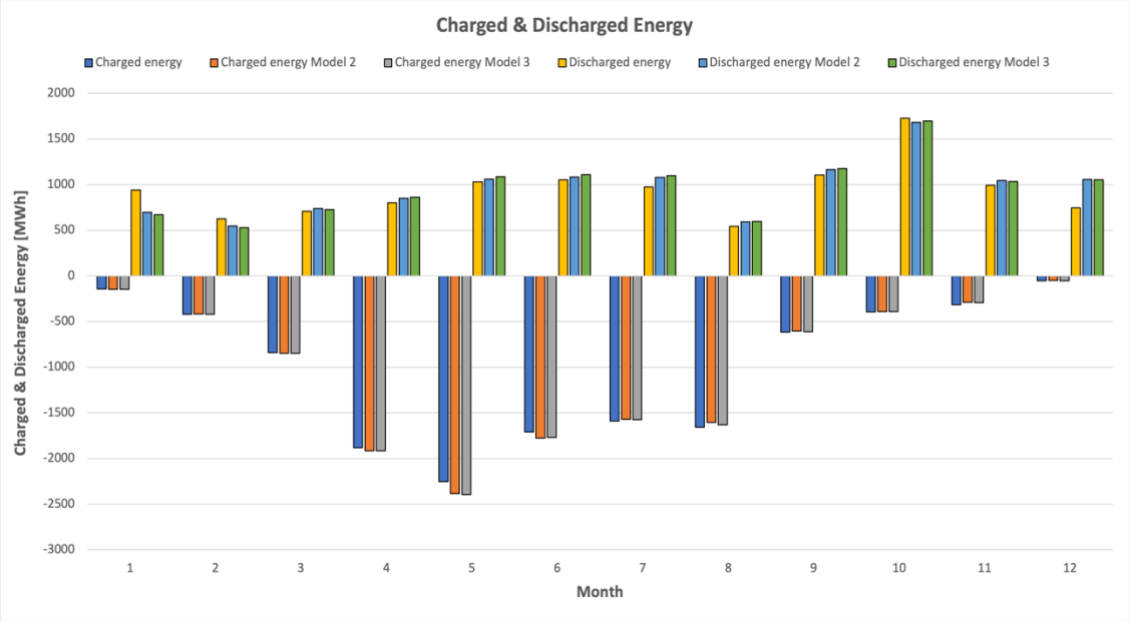

Figure 19. Comparison of monthly charged and discharged energy from Models 2 and 3

The fact that the charged energy shows an increasing trend can be seen in Table 10, where the charged energy from the main port, i.e. when the top and bottom diffusers work simultaneously, increases with each model developed. This may be caused by two reasons, either the top layer presents an increase on its temperature or the bottom layer decreases its temperature, both of reasons in a slight way. The total discharged energy is still overestimated due to the discharge operating condition when the water is going into the storage through the bottom diffuser and going out through the middle diffuser. While the deviation of the charged energy between the experimental data and simulation remains around -1%, discharged energy deviation increases with a value of -3% in Model 2 and -4% in Model 3.

Condition	Top – Bottom	Top – Middle	Middle - Bottom
Charge			
Measurement [MWh]	9565	973	1584
Model 2 [MWh]	9782	901	1576
Error (%)	-2	7	1
Model 3 [MWh]	9827	885	1591
Error (%)	-3	9	0
Discharge			
Measurement [MWh]	9431	1181	891
Model 2 [MWh]	9123	1218	1519
Error (%)	3	-3	-70
Model 3 [MWh]	9117	1248	1545
Error (%)	3	-6	-73

Table 10. Values of charged and discharged energy according to different ports from Models 2 and 3

Model 2 and Model 3 monthly heat losses and their total values are displayed in Figures 20 and 21 and Tables 11 and 12, respectively. The decrease of total heat losses according to the increase of the number of layers can be justified just by looking the total values within the period when the heat losses are higher, i.e. from April to August. In all models the highest value of heat losses takes place in August because it is the last month within the global charging period and the tank has been increasing its temperature during 5 months. Model 3 has the lowest highest value among the rest of the models.

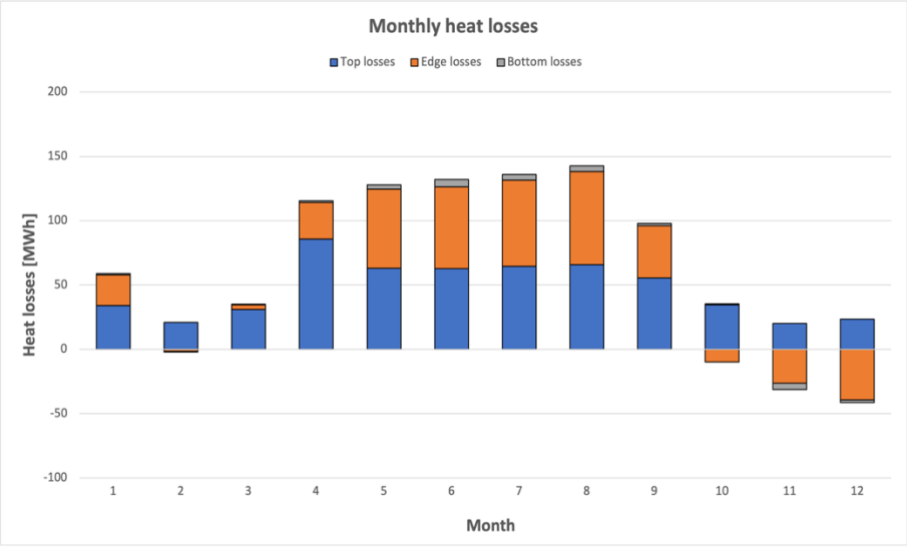

Figure 20. Annual evolution of heat losses from Model 2

Month	1	2	3	4	5	6	7	8	9	10	11	12
Losses [MWh]	59	19	35	115	128	132	136	143	98	25	-11	-19

Table 11. Monthly total heat losses from Model 2

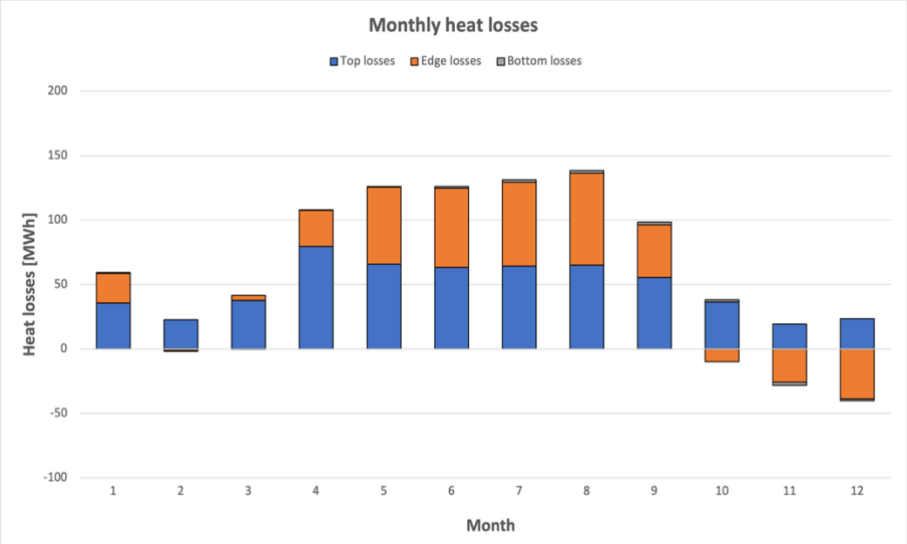

Figure 21. Annual evolution of heat losses from Model 3

Month	1	2	3	4	5	6	7	8	9	10	11	12
Losses [MWh]	59	21	42	108	126	126	131	138	98	28	-9	-17

Table 12. Monthly total heat losses from Model 3

In this section, the MIX number efficiency is going to be analyzed only for Model 2 (Figure 22) due to the MIX number computational difficulty when the number of layers keep increasing. The conclusion to be drawn with the 32 layer model is considered sufficient for models that can be discretized with a larger number of nodes. Anyway, the stratification coefficient is analyzed for both models, which means that more information about the thermal stratification of the storage is obtained when the model is formed by 48 layers. Focusing on the efficiency of the MIX number of Model 2, the evolution during the year is similar to that of Model 1, even reaching similar maximum and minimum values, respectively around 0.4 and 0.1. Even though its low values, the storage is still charging efficiently when global charging operation condition starts since it is when the highest value of the efficiency is reached.

According to the stratification coefficient, Model 3 reaches higher values than Model 2 and actual data, which means the storage is better stratified when the number of nodes is larger. The highest spikes on Figure 23 take place within the charging period, which means the temperature of the storage is not similar between layers and the PTES is highly stratified. By cons, during the final of the charge period, Model 2 values are closer or even below the curve of the actual data while Model 3 is mainly above the experimental results. This affirms that Model 3 has better thermal stratification during the whole charge period than Model 2 and experimental data. During the discharge period, both models are inefficiently operated because the total energy discharged is still overestimated and therefore the thermal stratification is low because the temperatures of each layer are closer to a uniform global temperature.

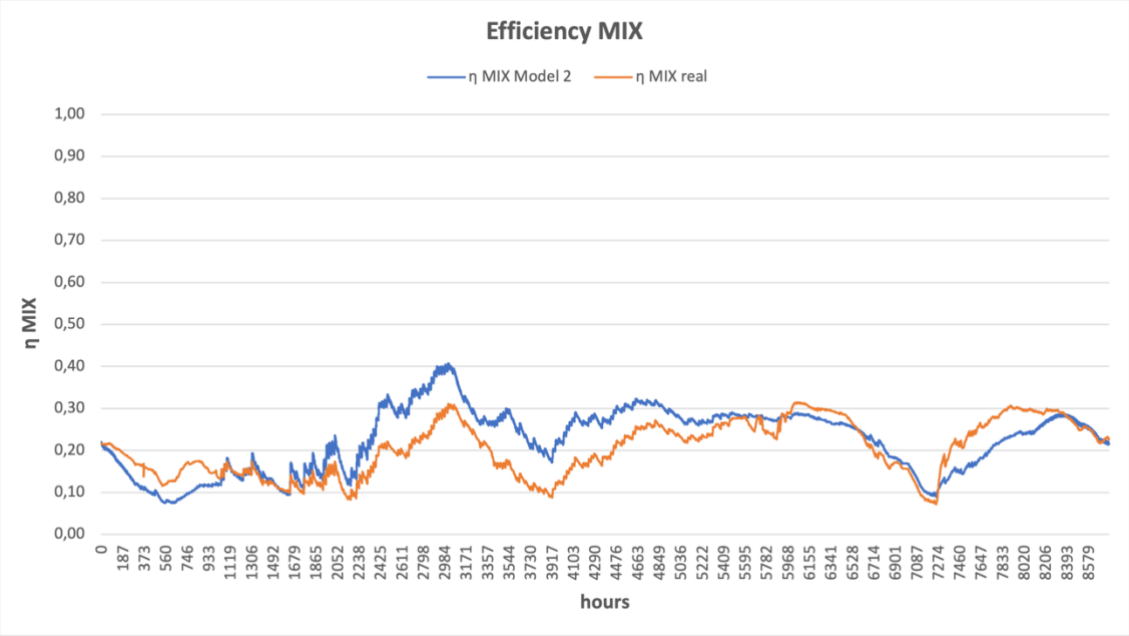

Figure 22. Annual evolution of the MIX number efficiency from Model 2

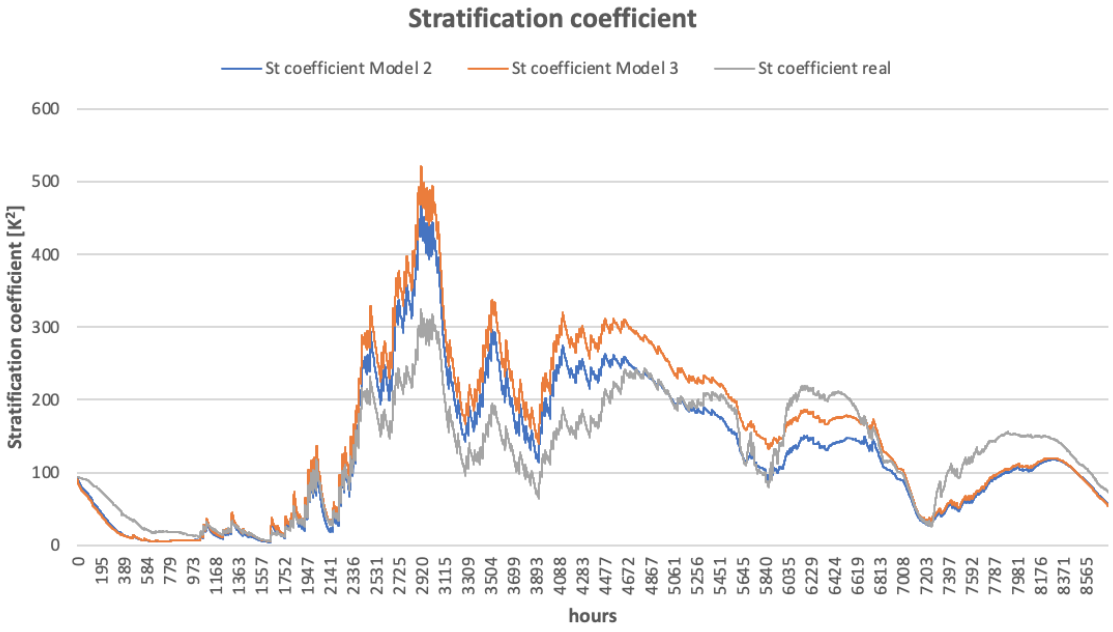

Figure 23. Annual evolution of the stratification coefficient from Models 2 and 3

9. Geometry changes evaluation – Model 4

In this section it is decided to keep both top and bottom surfaces with the same value than the real storage in order to see whether this geometrical change has some effect on the performance of the storage or not. Using equations *(44)*, *(45)* and *(46)* with its corresponding values, geometrical parameters are set on Table 14. It has to be taken into account that if the volume, height of the storage, top surface and bottom surface are to be kept constant according to the actual PTES, what it will change is the value of the slope. Indeed, the convection coefficients and heat transfer coefficients from the sidewall and bottom (Table 15) also change because they depend on the slope and the diameter of the bottom, according to equations *(17)*, *(18)*, *(19)* and *(20)*. This new model keeps it discretization of 32 layers like Model 2, so it is the one with it is going to be compared with.

Geometrical parameter	Value	Units
$A_{top,real}$	8100	m^2
$A_{top,\ model}$	8100	m^2
$A_{bottom,real}$	676	m^2
$A_{bottom,model}$	676	m^2
Volume	60000	m^3
Height	16	m
Slope	23.9	º
R_{top}	50.78	m
R_{bottom}	14.67	m

Table 13. Geometrical parameters of Model 4

Parameter	Bottom	Side
h [W/(m²·K)]	213	166
δ_{HDPE} [m]	$2.5 \cdot 10^{-3}$	$2.5 \cdot 10^{-3}$
λ_{HDPE} [W/(m·K)]	0.44	0.44
δ_{geo} [m]	$1 \cdot 10^{-3}$	$1 \cdot 10^{-3}$
λ_{geo} [W/(m·K)]	0.45	0.45
U [W/(m²·K)]	79.30	71.75

Table 14. Parameters for the Model 4 bottom and sidewall heat transfer coefficients calculation

All the results presented in Table 15 are practically the same than those from the Model 2 in Table 9. A slight difference can be appreciated on the total heat losses but it is only a difference of 13 MWh, which is considered negligible. Model 4 and Model 2 are equals according to the key parameters of the storage performance.

Parameter	Measurement data	Model 4
Charged energy [MWh]	11868	11997
Discharged energy [MWh]	11250	11588
Internal energy change [MWh]	-539	-485
Maximum temperature [ºC]	84.4	86.3
Minimum temperature [ºC]	8.7	8.6
Thermal capacity [MWh]	5286	5430
Storage efficiency (%)	90	93
Total heat losses [MWh]	1157	874
Top heat losses [MWh]	580	569
Edge heat losses [MWh]	-	291
Bottom heat losses [MWh]	-	14

Table 15. Key parameters from Model 4

No significant differences can be seen in the graphs of diffusers outlet temperatures. At first glance, the evolution of these temperatures seems to be the same between Model 4 and Model 2. Whether there is in fact any significant difference, it will be appreciated with the coefficient of determination method in a later section. The same applies for the average temperature of the storage. In any case, the graphs are presented in this section even though they are almost identical to the graphs of Model 2.

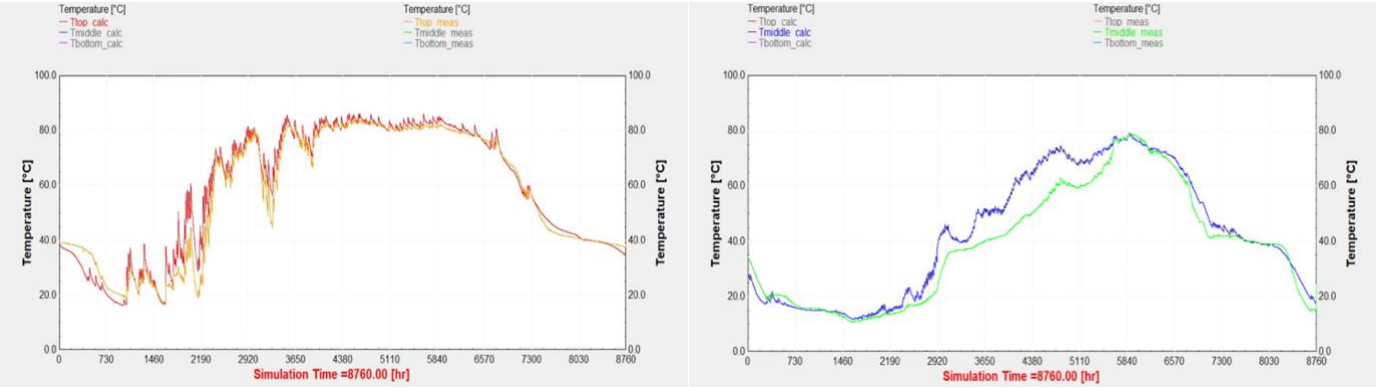

Figure 24. Comparison of the evolution of top and middle diffusers outlet temperature from Model 4

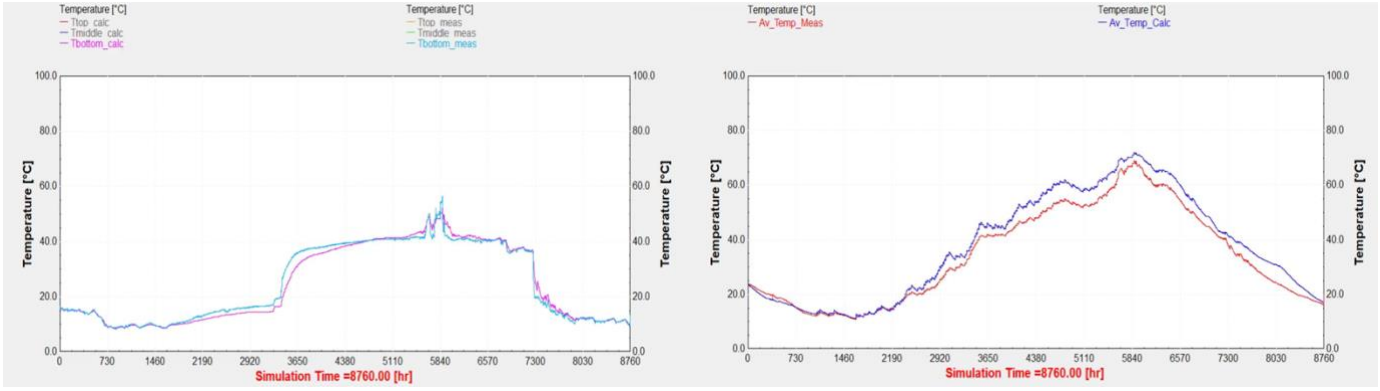

Figure 25. Comparison of the evolution of bottom diffuser outlet temperature and the average temperature from Model 4

For both the analysis of the charged and discharged energy and heat losses no observation is made in this respect, since Model 4 behaves the same as Model 2, even presenting the same or very similar values of the deviation from the experimental data. Anyhow, all the graphics and tables are presented in this report.

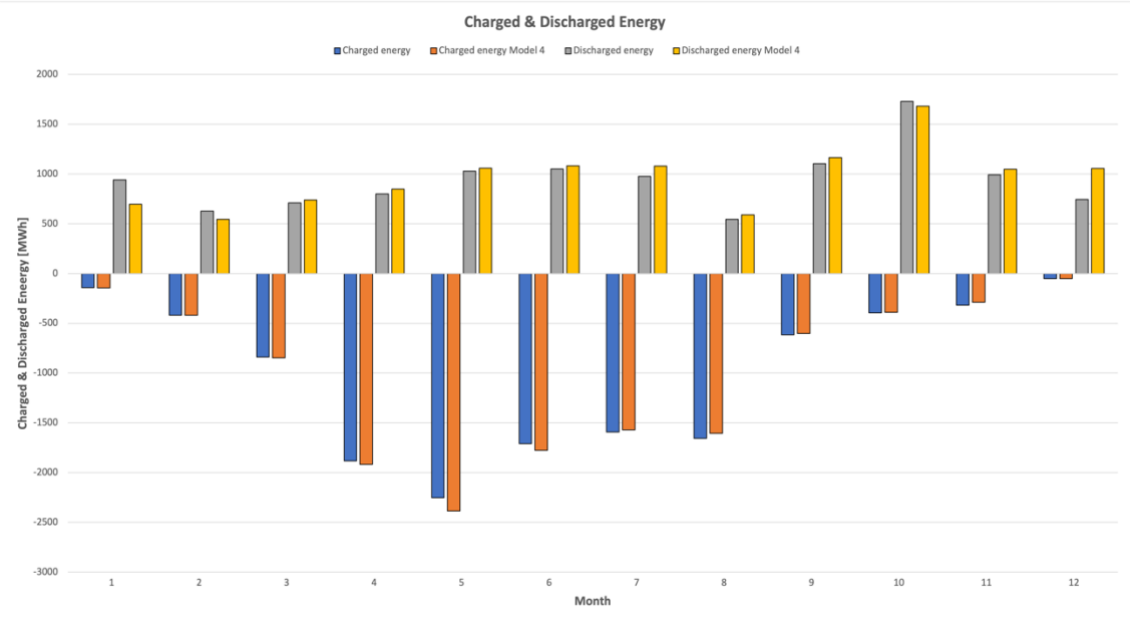

Figure 26. Comparison of monthly charged and discharged energy from Model 4

Condition	Top – Bottom	Top – Middle	Middle - Bottom
Charge			
Measurement [MWh]	9565	973	1584
Model 4 [MWh]	9827	885	1591
Error (%)	-3	9	0
Discharge			
Measurement [MWh]	9431	1181	891
Model 4 [MWh]	9117	1248	1545
Error (%)	3	-6	-73

Table 16. Values of charged and discharged energy according to different ports from Model 4

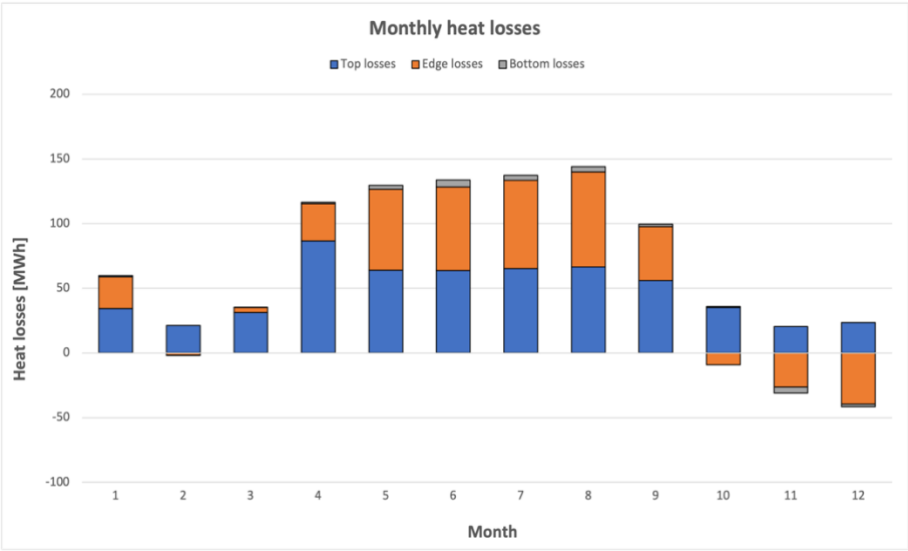

Figure 27. Annual evolution of heat losses from Model 4

Month	1	2	3	4	5	6	7	8	9	10	11	12
Losses [MWh]	60	19	35	117	130	134	137	144	100	26	-11	-18

Table 17. Monthly total heat losses from Model 4

The same applies for the thermal stratification, since even the maximum, minimum and average values of both stratification indicators are almost the same than in Model 2.

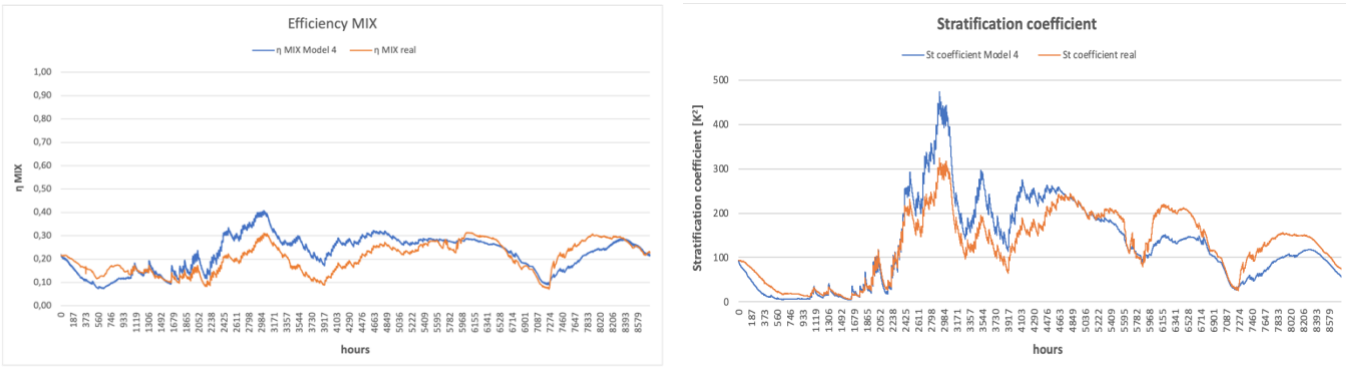

Figure 28. Annual evolution of the MIX number efficiency and the stratification coefficient from Model 4

10. Soil modifications – Model 5

Since this project is based on the study of two main TRNSYS elements developed by TESS, it is also interesting not only focus on the element based on the storage but also on the element that models the surrounding soil. The problem is that in this project it has not been possible to go as much depth as desired due to several impediments. To precisely know how this element works and in which way affects the storage it has been necessary to deep analyze its source code. It is the case that within this source code a series of subroutines are used and it has not been possible to access to this subroutines to know its precise development. As mentioned in section 6.2, the fact of not knowing the exactly mesh generation along vertical and radial axis has meant a lack of information. Type 1301 generates an output file that consists on the evolution of all the soil nodes temperatures but its format has been difficult to interpret and open with another more useful format as it is an unusual file, namely a file with an .OUT extension. Thus, a suggestion for further studies of the combination of both types is once the mesh is precisely well-known, analyze the evolution of the soil nodes temperatures along both axis and how it varies within the models described in previous sections or even changing another parameters of the soil type itself. For instance, this can be precisely analyzed with a software based on CFD as it can offer a clear overview of a region containing as much data as is generated in the output file created by type 1301.

It has also been found that the parameters offered by type 1301 are a bit lacking. For instance, it would be convenient to have the option to characterize with different parameters the two main kinds of soils that are present in the vicinity of the PTES. Since we can distinguish one soil mainly formed by dry sand and the deep-earth boundary is mainly formed by water saturated sand, this element do not allow to characterize this last type of soil and it will be interesting since the effect on the bottom of the storage could be studied by moving the vertical distance of the deep-earth boundary.

Since TRNSYS allows recompile the source code of existing elements, an user can make changes in the source code by using a FORTRAN compiler and modifying a .DLL file (Dynamic Link Library). This make it possible to make modifications that may be considered of interest for subsequent studies.

However, the model analyzed in this section consists of modifying the soil properties to study the possible advantages or disadvantages of building a PTES with the same characteristics as the Dronninglund PTES but in another location with a soil with different properties. The comparison with Model 2 is still maintained, which is divided into 32 layers.

In this case, a soil consisting of the same type of sand but with more water content is considered. According to some stated reports (Hamdhan et al., 2010 [16])(PlanEnergi, 2011 [8]), the properties of the new soil can be set at a density of 2100 kg/m^3, a specific heat of 1.16 kJ/(kg·K) and a thermal conductivity of 1.25 W/(m·K).

Table 18 shows that Model 5 has a very good accuracy in terms of discharged energy despite the amount of charged energy has a deviation of -3% while Model 2 has one of -1%, which means the energy delivered towards the inside of the storage is higher. The internal energy change suffers a drop and therefore it can be affirmed that the storage has a lower variation of temperature throughout the year in Model 5. The difference of around 30 MWh in terms of thermal capacity between Model 5 and Model 2 relies on the fact that the maximum temperature reached is 0.4 ºC lower.

Parameter	Measurement data	Model 5
Charged energy [MWh]	11868	12182
Discharged energy [MWh]	11250	11292
Internal energy change [MWh]	-539	-443
Maximum temperature [ºC]	84.4	85.9
Minimum temperature [ºC]	8.7	8.6
Thermal capacity [MWh]	5286	5399
Storage efficiency (%)	90	89
Total heat losses [MWh]	1157	1312
Top heat losses [MWh]	580	641
Edge heat losses [MWh]	-	640
Bottom heat losses [MWh]	-	31

Table 18. Key parameters from Model 5

The fact that neither the evolution nor the values of the three diffuser outlet temperatures nor the average temperature vary too much from one model to another means that no comments about them are made in this section, but will directly analyze their accuracy in a later section.

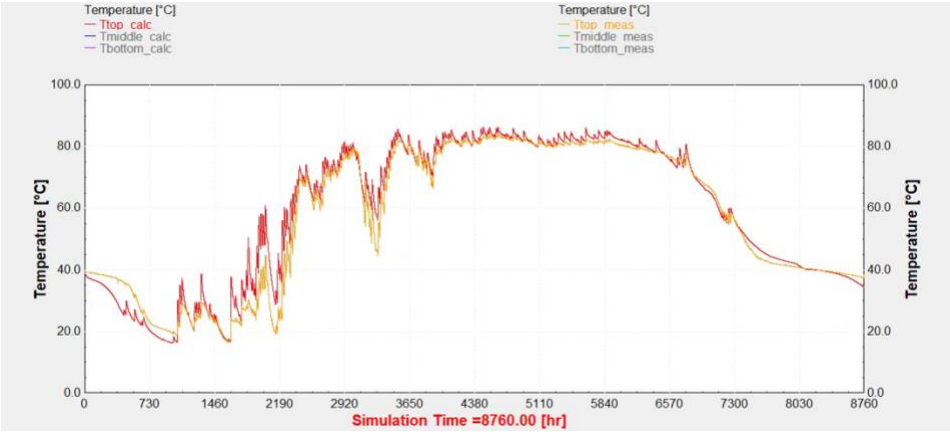

Figure 29. Comparison of the evolution of top diffuser outlet temperature from Model 5

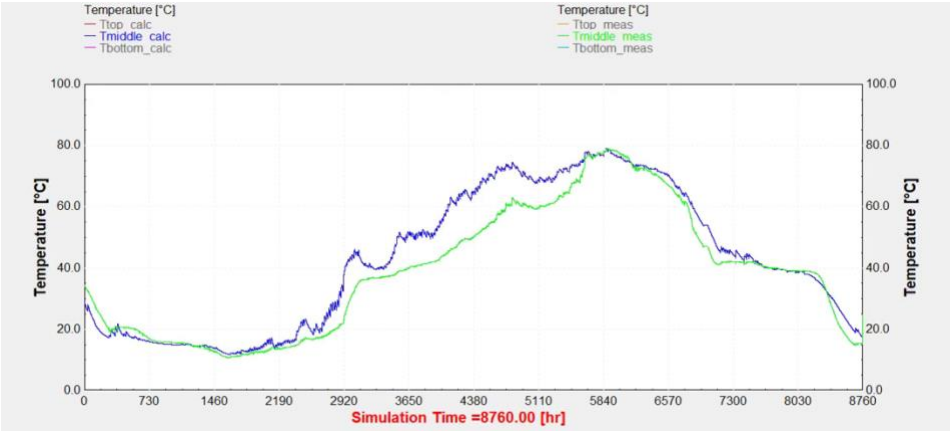

Figure 30. Comparison of the evolution of middle diffuser outlet temperature from Model 5

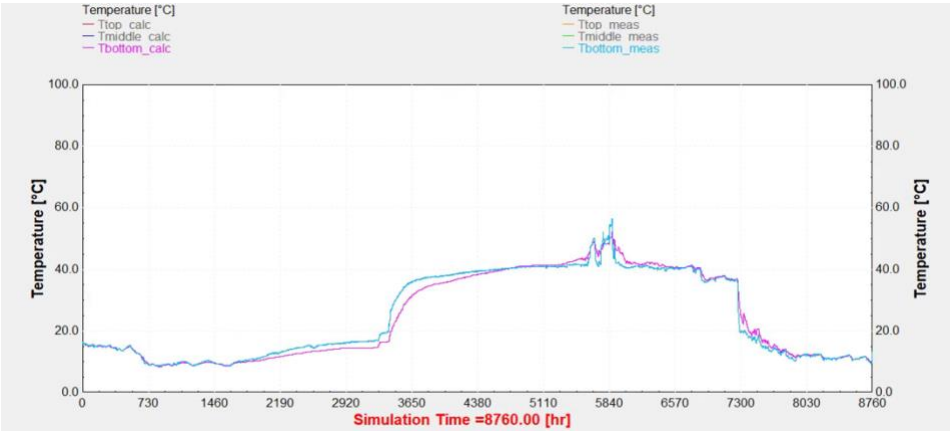

Figure 31. Comparison of the evolution of bottom diffuser outlet temperature from Model 5

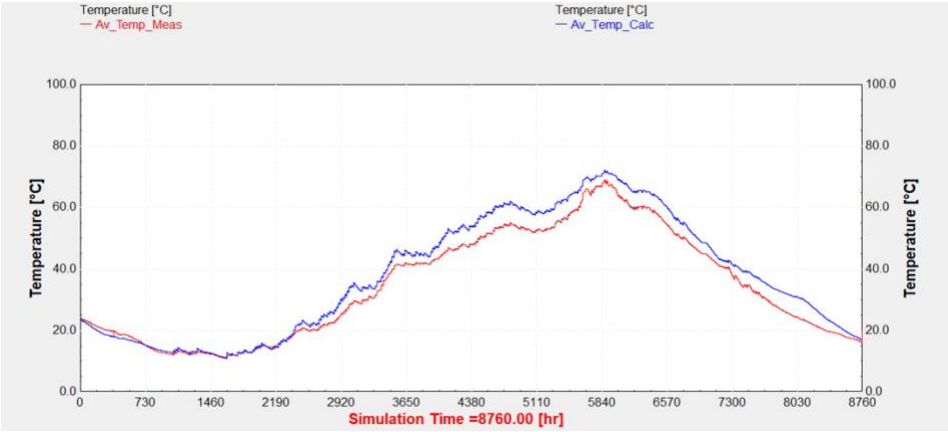

Figure 32. Comparison of the evolution of the average temperature from Model 5

As reflected in Figure 33, the annual evolution of charged and discharged energy is not only similar to Model 2, but also to the other models. A fact to take into account is that Model 5 is the one with the highest value (around 2400 MWh) of energy charged in the month in which the maximum occurs, i.e. in May. In this case, as in the case of the diffusers outlet temperatures and the average temperature of the storage, whether there is any significant difference will be seen with the analysis of the accuracy between the simulation and the experimental data. Checking Table 19, a noteworthy fact is that the port formed by the top and bottom diffusers, which has the most weight in terms of energy delivered, has the highest deviation in both charged and discharged energy, -4% and 6% respectively. The problem relies on the outlet temperatures since the rest of the parameters of the energy balance are already fixed. When it is charging period, the outlet temperature of the bottom diffuser is slightly higher than normal, maybe due to mixing. A similar effect occurs with the discharge process but the outlet temperature of the top diffuser leaves the storage with a slightly higher value.

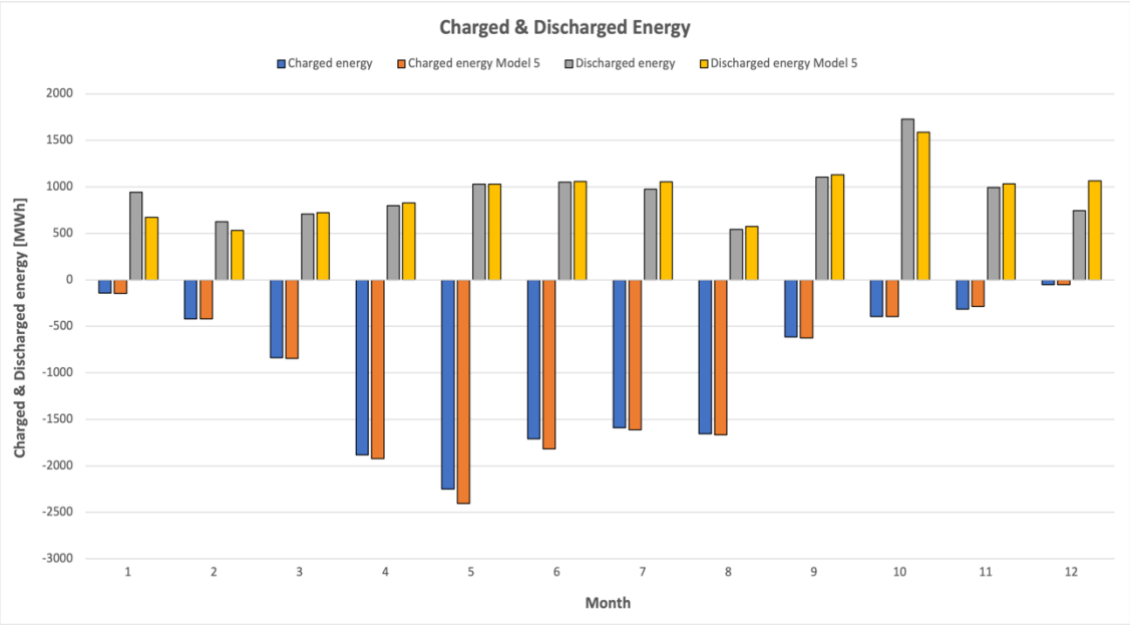

Figure 33. Comparison of monthly charged and discharged energy from Model 5

Condition	Top – Bottom	Top – Middle	Middle - Bottom
Charge			
Measurement [MWh]	9565	973	1584
Model 5 [MWh]	9921	919	1599
Error (%)	-4	6	-1
Discharge			
Measurement [MWh]	9431	1181	891
Model 5 [MWh]	8874	1175	1501
Error (%)	6	1	-68

Table 19. Values of charged and discharged energy according to different ports from Model 5

The main difference in heat losses is in the charging period (Figure 34). Due to the change in soil properties, the heat transfer between the tank wall and the adjacent soil is much higher than in other models. That is because the temperature of the soil closest to the sidewall has a lower temperature compared to the other models, whilst the temperature inside the storage maintains a more or less similar evolution among all the models. In general, this occurs not only in the area closest to the tank wall, but also in the top and bottom surface, since the total heat losses are greatly increased, precisely around 50%. Even the heat gain during the months of November and December is higher than in Model 2. The percentage distribution of the different types of heat losses is also modified with respect to all other models. While the percentage distribution was more or less 65%, 33% and 2% for top losses, edge losses and bottom losses respectively, with Model 5 this distribution changes completely even putting lid losses and edge losses at the same level with a loss of 48% loss over the total

each. Bottom losses suffer a small increase but their value remain low, with a 4% of the total heat losses. The difference in the month with the highest losses, i.e. August, is quite high at around 95 MWh.

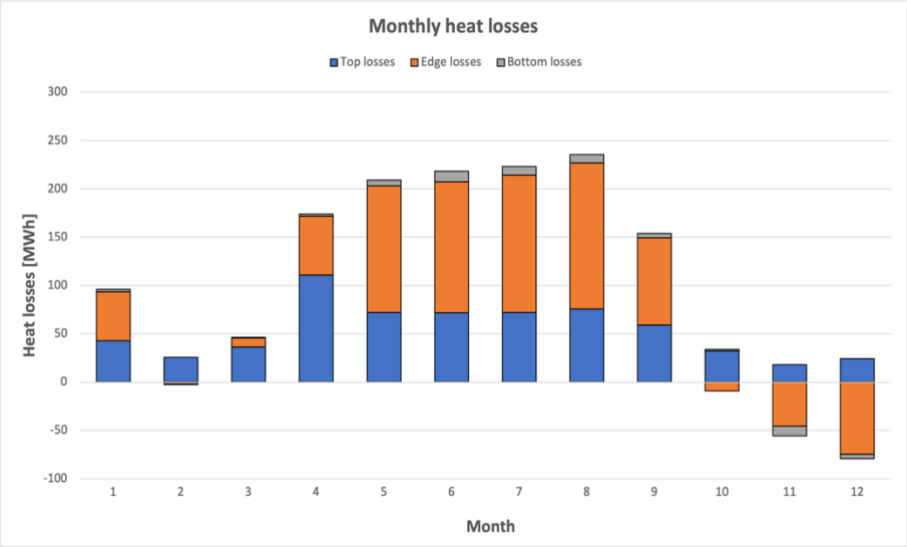

Figure 34. Annual evolution of heat losses from Model 5

Month	1	2	3	4	5	6	7	8	9	10	11	12
Losses [MWh]	96	23	46	174	209	218	223	236	154	25	-36	-55

Table 20. Monthly total heat losses from Model 5

The efficiency of the MIX number remains constant in comparison not only with Model 2 but also with the rest of the models (Figure 35). The stratification coefficient (Figure 36) shows the same behavior with an effectively realized charging period but within the period of switching the global operation condition and in the beginning of the discharge period this indicator suffers a decrease. A part from this, an improvement trend of the thermal stratification can be observed during the middle of the discharge period, but then it decreases again.

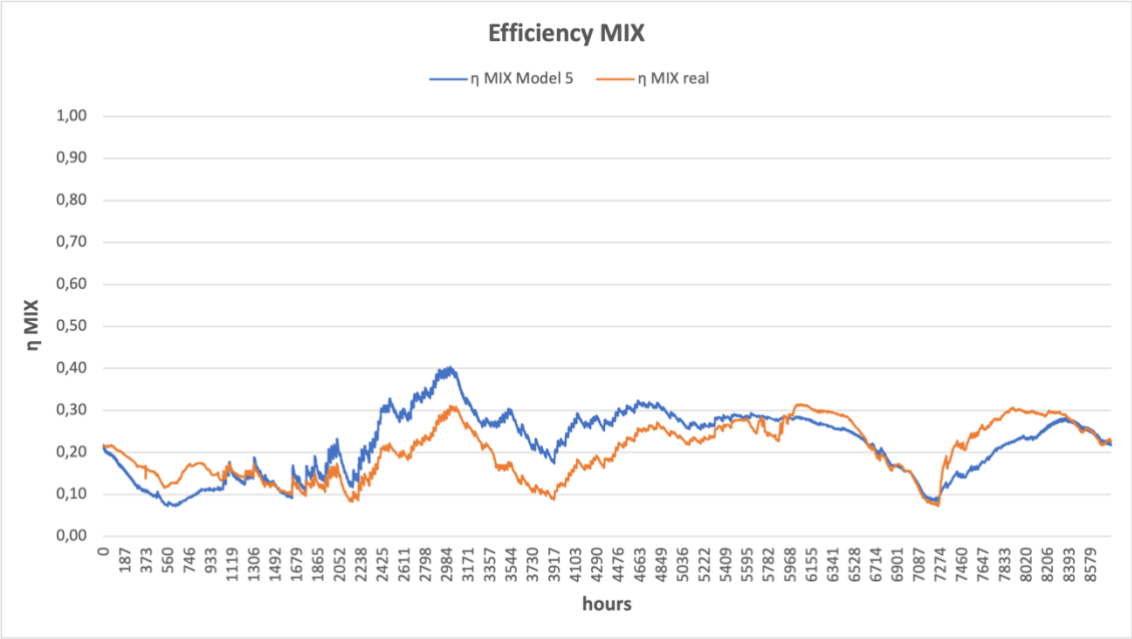

Figure 35. Annual evolution of the MIX number efficiency from Model 5

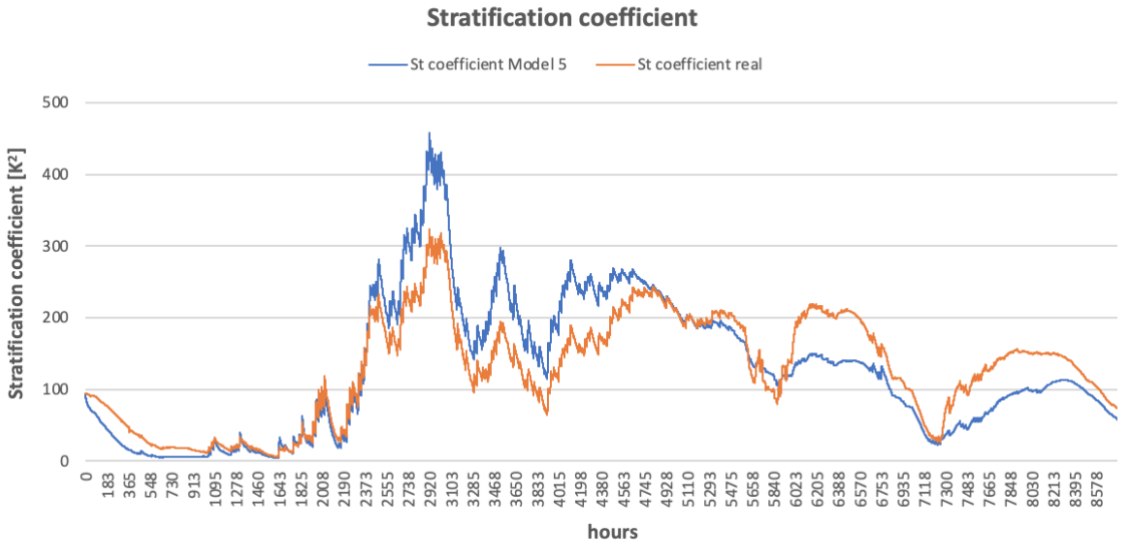

Figure 36. Annual evolution of the stratification coefficient from Model 5

11. Models accuracy

In addition to analyzing all the performance, efficiency and thermal stratification indicators of each model, the comparison of the accuracy of each model generated with respect to the experimental data is also an important objective of this project. As explained in section 4.1, the parameters to be studied using the coefficient of determination method are the three diffuser outlet temperatures and the charged and discharged energy. In Figure 37, the R^2 value of each model for the analysis parameter can be observed. The graph also includes the overall coefficient of determination to determine the total accuracy of each model, as described in equation *(8)*.

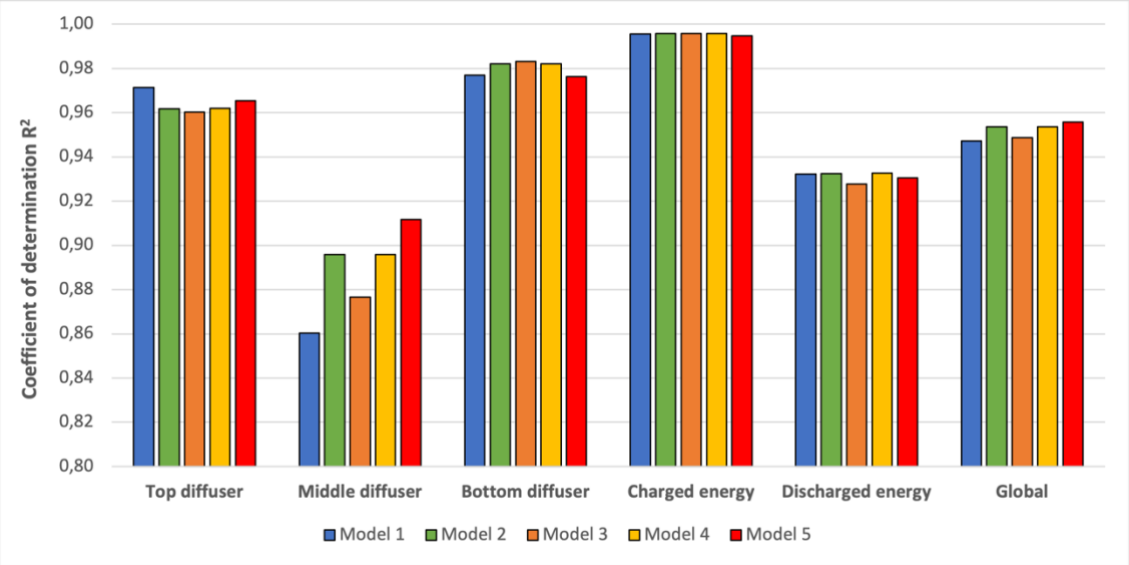

Figure 37. R^2 values of diffusers outlet temperatures, charged & discharged energy and global accuracy

The coefficient of determination of the top and bottom diffusers are pretty high for all the models, presenting higher values than 0.96 and even exceeding a value of 0.98 Models 2, 3 and 4 from the bottom diffuser outlet temperature. Not so good results can be observed in relation to the middle diffuser outlet temperature since only Model 5 exceeds a R^2 value of 0.9, while the others are within the range of 0.86 and 0.89. The models discretized with 32 layers (Model 2, 4 and 5) are the ones with higher R^2 values. This can rely on the location of the middle diffuser in the model, since it highly depends on the height of each layer. The largest error is produced in the charge period, being the outlet temperatures of the middle diffuser underestimated in all cases. The fact that the temperature of the water coming out from the middle diffuser is higher in Model 5 can be justified by the increase of the total heat losses, especially during the charge period. The accuracy of the amount of charged energy is

almost exact for all the models. By cons, the reason why the discharged energy is not as accurate as the charged one is because the fact that the discharged energy when middle and bottom diffuser are working simultaneously is heavily overestimated in all models, as it has been mentioned during the report. Nevertheless, the R^2 values of the discharged energy are acceptable because the error that is produced does not greatly affect the accuracy since the operating condition of the mentioned port is not really common during the year. Lastly, the best models according to the global R^2 value are Models 2, 4 and 5, the storages of which are divided into 32 layers. Model 5 shows a slightly higher value of the coefficient of determination than the other two models mainly due to the high accuracy of the outlet temperature of the middle diffuser compared to the rest of the models.

12. Conclusions

The overall and thermal performance of the PTES of Dronninglund SDH plant is really important to analyze in order to obtain useful information for further studies. In this project, several models are developed with TRNSYS using type 1535 and type 1301 as main elements. The aim of the project is to observe how modifications in the discretization of the water pit heat storage, changes in geometric parameters and consideration of different types of surrounding soils affect the energy delivered by the storage (charged and charged), diffuser outlet temperatures, heat losses from the envelope of the storage and the tank thermal stratification. After an in-depth study of all the models, the following conclusions can be drawn.

According to the global R^2 value, the best models in terms of accuracy are the ones in which the storage is divided into 32 layers, i.e. Models 2, 4 and 5. The fact that the best model is the one with a soil considered water-saturated is a bit misleading because in terms of heat losses is overestimated with a deviation of 15%.

The experimental annual charged energy is 11868 MWh and the discharged energy is 11250 MWh. In terms of charged energy, all models are highly accurate with a deviation of -1% except Model 5 that has a deviation of -3%, but still considered low. Considering discharged energy, models are not as accurate due to the overestimated discharge operation of the middle and bottom diffusers working simultaneously. However, as it is not a common operating condition, the deviation between the models and the simulation is still low. It also has to be said that it would be convenient to study in depth why is produced this surplus of discharged energy and find the focus of the problem, whether it comes from an error of the experimental data or from the model performance.

Both top and bottom diffuser outlet temperatures of all models are really accurate. On the other hand, an underestimated behavior of the middle diffuser outlet temperature during the global charge period is observed in all models. This may be due to the not really adequate location of the middle diffuser in the models according to the position of this diffuser in the real storage. This may also be due to a computational problem in the simulations, since during the overall charging period the temperature of the geometric center zone of the storage is slightly lower than that of the experimental data. The same applies for the average

temperature of the storage, which its deviation respect to the actual average temperature can be caused by the problems discussed above.

Total heat losses of all models are underestimated compared to the experimental heat losses obtained by an energy balance, except the heat losses of Model 5, which are overestimated. Their value highly dependent on the value of the heat transfer coefficients of the top, edge and bottom surfaces. Since in this project they are calculated manually and somewhat archaic, it may be interesting to use some optimization tools to obtain values that more closely resemble reality, for example GenOpt, which has been used in another studies (Gauthier, 2020 [5]).

Attending to the thermal stratification of the storage, the conclusions that can be drawn are not very good. MIX number efficiency is quite low throughout the year in all models, reaching values under 50%, which indicates that the storage is closer to be fully mixed than perfectly stratified. However, it has to be said that due to the difficulty of calculation and the large number of parameters on which this indicator depends, the assessment of the thermal stratification is not very reliable. The stratification coefficient provides a little more information between models since the more layers the storage has, the higher the values of this indicator, which indicates better stratification. Another fact that has been observed is that during the switch of the global operation condition from discharge to charge in April, the storage is charged efficiently since this is when the highest values of both indicators are reached. On the other hand, as heat losses increase during the charge period, the tank suffers a decrease in its thermal stratification, which also occurs when the operation condition changes again, but in this case from charge to discharge.

To conclude, this study can be a good starting point for future investigations of type 1535 and type 1301 working simultaneously in a TRNSYS model. Several aspects that have been discussed during the course of the project can be further elaborated upon, but with a good basis of support using this study.

References

[1] Danish Energy Agency, Danish Ministry of Climate, Energy and Utilities. Heat. https://ens.dk/en/our-responsibilities/heat

[2] Tulus, V., Boer, D., Cabeza, L.F., Jiménez, L., Guillén-Gosálbez, G., 2016. Enhanced thermal energy supply via central solar heating plants with seasonal storage: A multi-objective optimization approach. Appl. Energy 181, 549-561. https://doi.org/10.1016/j.apenergy.2016.08.037

[3] Ochs, F., Heidemann, W., Müller-Steinhagen, H., 2009. Performance of Large-scale seasonal thermal energy stores. J. Sol. Energy Eng. Trans. ASME 131, 0410051–0410057. https://doi.org/10.1115/1.3197842

[4] Dahash, A., Ochs, F., Janetti, M.B., Streicher, W., 2019b. Advances in seasonal thermal energy storage for solar district heating applications: A critical review on large-scale hot-water tank and pit thermal energy storage systems. Appl. Energy 239, 296–315. https://doi.org/10.1016/j.apenergy.2019.01.189

[5] Gauthier, G., 2020: Benchmarking and improving models of subsurface heat storage dynamics. Comparison of Danish PTES and BTES installation measurements with their corresponding TRNSYS models. GEOTHERMICA - ERA NET Cofund Geothermal. 47 pp.

[6] Xie, Z., Xiang, Y., Wang, D., Kusyy, O., Kong, W., Furbo, S., Fan, J., 2021. Numerical investigations of long-term thermal performance of a large water pit heat storage. Sol. Energy 224, 808–822. https://doi.org/10.1016/j.solener.2021.06.027

[7] PlanEnergi, 2015. SUNSTORE 3 Phase 2 Implementation.

[8] PlanEnergi, 2011. SUNSTORE 3. Phase 1: Projektering og udbud.

[9] Jensen, M.V., 2014. Task 45 Large Systems Seasonal pit heat storages - Guidelines for materials & construction, IEA-SHC TECH SHEET 45.B.3.2.

[10] Haller, M.Y., Cruickshank, C.A., Streicher, W., Harrison, S.J., Andersen, E., Furbo, S., 2009. Methods to determine stratification efficiency of thermal energy storage processes - Review and theoretical comparison. Sol. Energy 83, 1847–1860. https://doi.org/10.1016/j.solener.2009.06.019

[11] Andersen, E., Furbo, S., Fan, J., 2007. Multilayer fabric stratification pipes for solar tanks. Sol. Energy 81, 1219–1226. https://doi.org/10.1016/j.solener.2007.01.008

[12] Wu, L., Bannerot, R.B., 1987. An experimental study of the effect of water extraction on thermal stratification in storage, in: Proceedings of the 1987 ASME-JSME-JSES Solar Energy Conference, Honolulu. pp. 445–451.

[13] Bergman, T.L., Incropera, F.P., DeWitt, D.P., Lavine, A.S., 2011. Fundamentals of heat and massctransfer. John Wiley & Sons.

[14] Ochs, F., 2009. Modelling Large-Scale Thermal Energy Stores. Shaker Verlag, Stuttgart,Germany.

[15] Forkel, C., Daniels, H., 1995. Finite element simulation of circulation in large scale thermal energy storage basins. Adv. Water Resour. 18, 147–158.

[16] Hamdhan, I.N., Clarke, B.G., 2010. Determination of Thermal Conductivity of Coarse and Fine Sand Soils, in: Proceedings World Geothermal Congress.

[17] Kusuda, T. and P.R. Achenbach. 1965. 'Earth Temperatures and Thermal Diffusivity at Selected Stations in the United States.' *ASHRAE Transactions*. 71(1): 61-74.

[18] Climate-Data. https://en.climate-data.org/europe/denmark/north-denmark-region/dronninglund-770718/